Bachelor thesis at the Institute of Mathematics of Freie Universität Berlin,

Research Group Numerical Mathematics and Scientific Computing

The Smagorinsky turbulence model

Marco Rösler
Student number: 4460910
MarcoDRoesler@icloud.com

Supervisor: Prof. Dr. Volker John*
Second assessor: Dr. Naveed Ahmed†

Berlin, May 13, 2015

Abstract

This bachelor thesis considers the Smagorinsky turbulence model and its derivation. The model is used to simulate turbulent flows around a surface mounted cube in a rectangular channel with the code MooNMD. Emphasis is placed on the lift and drag force on the cube and the respective coefficients. The numerical results of the mean drag coefficients for different choices of the turbulent viscosity constant are compared to some other studies that consider this benchmark problem.

*https://www.wias-berlin.de/people/john/
†https://www.wias-berlin.de/~ahmed/

Author's Declaration of Originality

I hereby declare that this thesis is my original work and it has been written by me in its entirety. I have acknowledged all the sources of information which have been used in the thesis. This thesis has not been submitted to any other University or Institution.

May 13, 2015

Marco Rösler

Contents

1 Introduction

1.1 Overview

Section 1 gives a short introduction to turbulent flows. Subsection 1.5 explains the difficulties in the simulation of turbulent flows.
Section 2 introduces large-eddy simulations (LES) and the Smagorinsky model. The derivation and mathematical aspects of the model are discussed.
Section 3 presents numerical studies: Turbulent flow around a cube was simulated using the Smagorinsky model. Various formulas for the lift and drag coefficients of the cube are derived. The lift and drag coefficients from the simulations are compared to other studies.
In Section 4, the major results and conclusions are summarized.
Additional information can be found in the Appendix.

1.2 Notation

If not otherwise specified, the Einstein notation is used. Angle brackets mean a statistical average. ∂_i is a shorthand for $\frac{\partial}{\partial x_i}$ and ∂_t for $\frac{\partial}{\partial t}$. See p. 38 for the nomenclature.

1.3 Turbulent flows

Turbulent flows can be encountered in nature and as a result of the work of man, such as a river or the smoke from a chimney. The study of such flows is important for aeronautics, meteorology and engineering, among others.
The Reynolds number

$$\mathrm{Re} = \frac{UL}{\nu} = \frac{\rho UL}{\mu} \tag{1.1}$$

(with characteristic velocity U, characteristic length L, kinematic viscosity ν, density ρ and dynamic viscosity μ) is a measure for the turbulence of a flow. Reynolds' pipe-flow experiment for example, a flow with a Reynolds number above 4000, is turbulent [1, p. 6].

1.4 Navier-Stokes equations

In this bachelor thesis the Navier-Stokes equations (NSE) play a central role as they describe the motion of fluids. For incompressible and homogeneous fluids[1], they are given as

$$\partial_t u_j + u_i \partial_i u_j = 2\nu \partial_i S_{ij} - \frac{1}{\rho}\partial_j P + f_j \quad \text{in } \Omega \times (0,T], \quad j = 1,2,3, \tag{1.2}$$

$$\partial_i u_i = 0 \quad \text{in } \Omega \times [0,T], \tag{1.3}$$

[1] A fluid is incompressible if the density remains constant and homogeneous if the viscosity is constant. Both is always assumed in this thesis.

where $\mathbf{u}(\mathbf{x},t) = (u_1, u_2, u_3)(\mathbf{x},t)$ is the velocity field depending on the position in space and time, ν the kinematic velocity,

$$S_{ij} = S_{ij}(\mathbf{u}) := \frac{1}{2}\left(\partial_i u_j + \partial_j u_i\right) \tag{1.4}$$

the rate-of-strain tensor representing friction between particles [2, p. 12], $\mathbf{f} = (f_1, f_2, f_3)$ forces per unit mass acting on the fluid, ρ the density of the fluid, P the pressure, $(0,T]$ and $[0,T]$ time intervals and $\Omega \subseteq \mathbb{R}^3$ the domain [1, pp. 14-17]. The momentum equation (Eq. (1.2)) is based on the conservation of momentum and the continuity equation (Eq. (1.3)) on the conservation of mass.

1.5 Problems simulating turbulent flows

The assumptions that led to the NSE are well-founded, but we are nevertheless working with a model. One difficulty is the coupling of the velocity and pressure and another the non-linearity of the convective term $u_i\partial_i u_j$ [2, p. 15].
Numerically solving the NSE in the case of turbulent flows is difficult because of the vastness of the information that is contained in the velocity field. The equations can be solved with direct numerical simulations (DNS), but the computational cost is a rapidly increasing (polynomial) function of the Reynolds number [1, pp. 339 and 349]. For example, a DNS of a turbulent flow at $\mathrm{Re} = 10^6$ would require $\mathrm{Re}^3 = 10^{18}$ uniformly distributed mesh points in space-time [3]. Thus, those calculations with very high Reynolds numbers are not even feasible in the near future, despite Moore's law.
A method other than DNS of non-averaged values is to focus on the mean values, a statistical approach. A large-eddy simulation (LES), which can be implemented using the Smagorinsky model, is such an approach. It is cheaper than DNS and seeks to alleviate the limitations of DNS by only explicitly computing the dynamics of the larger-scale motions and representing the influence of smaller scales through simple models [1, p. 558].

2 Fundamentals

2.1 Introduction to large-eddy simulations

In large-eddy simulations (LES) large-scale motions are represented directly and smaller-scale motions are modeled. Pope [1, pp. 558f.] mentions four conceptual steps:

1. The velocity $\mathbf{u}$ is split between a filtered component $\overline{\mathbf{u}}$ and a residual (subgrid-scale) component $\mathbf{u}' = \mathbf{u} - \overline{\mathbf{u}}$. The former represents the motion of large eddies.

2. In order to compute the evolution of the filtered velocity field, the filtered Navier-Stokes equations are derived from the Navier-Stokes equations (NSE). They have the same form as the unfiltered Navier-Stokes equations except a residual stress tensor arising from the residual motions.

3. The residual stress tensor has to be modeled in order to achieve closure of the equations.

4. The filtered equations are then solved numerically for the filtered velocity.

The filtering operation is defined as

$$\overline{\mathbf{u}}(\mathbf{x},t) := \int G_\Delta(\mathbf{r},\mathbf{x})\,\mathbf{u}(\mathbf{x}-\mathbf{r},t)\,d\mathbf{r}$$

with integration over the flow domain and the filter function G_Δ (often dependent on the filter width Δ) satisfying the normalization condition

$$\int G_\Delta(\mathbf{r},\mathbf{x})\,d\mathbf{r} = 1$$

[1, pp. 561f.]. If not otherwise defined, an overline on a variable denotes a filtered value.
A filter is called uniform if G_Δ does not depend on $\mathbf{x}$, and isotropic if G_Δ depends on $\mathbf{r}$ only through $r = |\mathbf{r}|$ [1, pp. 575f.].
It is easy to see that the filtering operation preserves constants and is linear. Filtering also commutes with differentiating with respect to time and it commutes with taking the mean [1, p. 562]. However, only certain filters commute with differentiating with respect to x_j [4, pp. 14f]. A common isotropic filter is a Gaussian

$$G_\Delta(\mathbf{r}) = \left(\frac{6}{\pi\Delta^2}\right)^{\frac{1}{2}} \exp\left(-\frac{6|\mathbf{r}|^2}{\Delta^2}\right)$$

[5, p. 996], [1, p. 563].
There are many different filter functions with different properties. We only consider filters who commute with differentiating.
Filtering the NSE (Eqs. (1.2) and (1.3)) yields:

$$\partial_t \overline{u}_j + \overline{u}_i \partial_i \overline{u}_j = \partial_i \left(2\nu \overline{S}_{ij} - \tau^r_{ij}\right) - \partial_j \bar{p} + \overline{f}_j \quad \text{in } \Omega \times (0,T], \quad j = 1,2,3, \tag{2.1}$$

$$\partial_i \overline{u}_i = 0 \qquad \text{in } \Omega \times [0,T]. \tag{2.2}$$

While the derivation of the filtered continuity equation is trivial, the derivation of the filtered momentum equation requires some work (see Section 5.A). The anisotropic residual-stress tensor τ^r_{ij} (Eq. (5.2)) and the modified filtered pressure $\bar{p}$ (Eq. (5.3)) were introduced to achieve a resemblance to the unfiltered momentum equation (Eq. (1.2)).

2.2 The Smagorinsky model

In order to close the equations and thereby determine the filtered velocity field $\overline{\mathbf{u}}(\mathbf{x},t)$ and the modified filtered pressure $\bar{p}(\mathbf{x},t)$, we need to model the anisotropic residual-stress tensor $\tau^r_{ij}(\mathbf{x},t)$. The Smagorinsky model[2] is the most simple model and has been proven to perform reasonably well [1, pp. 587-603].
In this model, the anisotropic residual-stress tensor τ^r_{ij} is related to the filtered rate-of-strain

$$\overline{S}_{ij} = \overline{S}_{ij}(\mathbf{u}) := S_{ij}(\overline{\mathbf{u}}) = \frac{1}{2}\left(\partial_j \overline{u}_i + \partial_i \overline{u}_j\right) \tag{2.3}$$

as

$$\tau^r_{ij} = -2\nu_r \overline{S}_{ij} \tag{2.4}$$

[1, p. 587], [6, p. 48]. This is the mathematical realization of the Boussinesq hypothesis, that turbulent fluctuations are dissipative in the mean [7, p. 74]. The mathematical structure is similar to that of molecular diffusion [4, p. 81]. Substituting Eq. (2.4) into Eq. (2.1), the filtered momentum equation can be written as

$$\partial_t \overline{u}_j + \overline{u}_i \partial_i \overline{u}_j = 2\,\partial_i \left((\nu + \nu_r)\overline{S}_{ij}\right) - \partial_j \bar{p} + \overline{f}_j, \qquad j = 1,2,3.$$

The residual subgrid-scale eddy viscosity ν_r acts as an artificial viscosity [6, p. 48] and represents the eddy viscosity of the residual motions. It is modeled as

$$\nu_r = \ell_S^2 \left(2\overline{S}_{lk}\overline{S}_{lk}\right)^{\frac{1}{2}} = (C_S \Delta)^2 \left(2\overline{S}_{lk}\overline{S}_{lk}\right)^{\frac{1}{2}} \tag{2.5}$$

[2] Named after American meteorologist Joseph Smagorinsky. It is also known as the Smagorinsky-Lilly model after his colleague Douglas Lilly.

[1, p. 587], [4, p. 95]. Here, we have the Smagorinsky lengthscale $\ell_S = C_S\Delta$, the Smagorinsky coefficient C_S and the filter width Δ.
Finally, we can write the filtered momentum equation as

$$\partial_t \overline{u}_j + \overline{u}_i \partial_i \overline{u}_j = 2\,\partial_i \left(\left(\nu + \ell_S^2 \left(2\overline{S}_{lk}\overline{S}_{lk} \right)^{\frac{1}{2}} \right) \overline{S}_{ij} \right) - \partial_j \bar{p} + \overline{f}_j, \quad j = 1,2,3.$$

The model for the eddy viscosity (Eq. (2.5)) is called Smagorinsky model, which is derived in Section 2.3.
The Smagorinsky model has some drawbacks. They are summarized as follows in [6, p. 49]:

- "The Smagorinsky model constant C_S is an a priori input. This single constant is incapable to represent correctly various turbulent flows.
- The eddy viscosity does not vanish for a laminar flow.
- The backscatter of energy is prevented completely since

$$(C_S\Delta)^2 \left(2\overline{S}_{lk}\overline{S}_{lk} \right)^{\frac{1}{2}} \geq 0.$$

- The Smagorinsky model introduces, in general, too much diffusion into the flow.[3]"

2.3 Derivation of the Smagorinsky model

According to [9, p. 279], the Smagorinsky model "can be derived in a number of ways including heuristic methods, for example, by equating production and dissipation of subgrid-scale turbulent kinetic energy, or via turbulence theories." A derivation that was adapted from [4] is shown here. Both heuristic methods and turbulent theories are taken into consideration.
Kolmogorov [10] (cited in [7, pp. 44-46]) derived the universal form of the energy spectrum function

$$E(k) = K\langle\varepsilon\rangle^{\frac{2}{3}} k^{-\frac{5}{3}}, \quad K \approx 1.4, \tag{2.6}$$

where

$$\varepsilon(t) := \frac{\nu}{|\Omega|} \int_\Omega |\nabla \mathbf{u}|^2(\mathbf{x}, t)\, d\mathbf{x} \tag{2.7}$$

is the energy dissipation rate, K a constant and angle brackets mean a statistical average. In short, this means that there is an energy cascade from the large scales to the smaller scales. This has been famously summarized in a poem by mathematician and meteorologist L. F. Richardson, as quoted in [7, p. 46]:

[3] The formula and the variables were adjusted to reflect this thesis' nomenclature. Note that the source cites [8].

> Big whirls have little whirls what feed on their velocity,
> little whirls have smaller whirls, and so on to viscosity.

Dimensional analysis shows that

$$\partial_i \tau_{ij}^r \left[\frac{\mathrm{m}}{\mathrm{s}^2}\right] \Leftrightarrow \tau_{ij}^r = -2\nu_r \overline{S}_{ij} \left[\frac{\mathrm{m}^2}{\mathrm{s}^2}\right] \Leftrightarrow \nu_r \left[\frac{\mathrm{m}^2}{\mathrm{s}}\right].$$

Therefore, it is assumed that the residual subgrid-scale eddy viscosity ν_r is proportional to $\tilde{\varepsilon}^{\frac{1}{3}}\Delta^{\frac{4}{3}}$, with $\tilde{\varepsilon}\ \left[\mathrm{m}^2/\mathrm{s}^3\right]$ the kinetic energy transfer rate [4, p. 85]. Using Eq. (2.6) and the so-called two-fluid model (TFM) or eddy-damped quasinormal Markovian (EDQNM) model, we get:

$$\langle \nu_r \rangle = \frac{A}{\pi^{4/3} K} \langle \tilde{\varepsilon} \rangle^{\frac{1}{3}} \Delta^{\frac{4}{3}}, \tag{2.8}$$

where A is a constant, which is is 0.438 according to the TFM and 0.441 according to the EDQNM theory [11] (as cited in [4, p. 85]).
Furthermore, in the isotropic homogeneous case,

$$\langle 2\overline{S}_{lk}\overline{S}_{lk} \rangle = \int_0^{\frac{\pi}{\Delta}} 2k^2 E(k)\, dk \tag{2.9}$$

is true [4, p. 85]. Substituting Eq. (2.6) into Eq. (2.9) yields

$$\begin{aligned}
\langle 2\overline{S}_{lk}\overline{S}_{lk} \rangle &= \int_0^{\frac{\pi}{\Delta}} 2k^2 K \langle \varepsilon \rangle^{\frac{2}{3}} k^{-\frac{5}{3}}\, dk \\
&= 2K \langle \varepsilon \rangle^{\frac{2}{3}} \int_0^{\frac{\pi}{\Delta}} k^{\frac{1}{3}}\, dk \\
&= \frac{3}{2} K \langle \varepsilon \rangle^{\frac{2}{3}} \pi^{\frac{4}{3}} \Delta^{-\frac{4}{3}}.
\end{aligned}$$

This is equivalent to

$$\begin{aligned}
\left(\frac{3K}{2}\right)^{\frac{3}{2}} \langle \varepsilon \rangle \pi^2 \Delta^{-2} &= \langle 2\overline{S}_{lk}\overline{S}_{lk} \rangle^{\frac{3}{2}} \\
\Longleftrightarrow \langle \varepsilon \rangle &= \frac{1}{\pi^2} \left(\frac{3K}{2}\right)^{-\frac{3}{2}} \Delta^2 \langle 2\overline{S}_{lk}\overline{S}_{lk} \rangle^{\frac{3}{2}}.
\end{aligned} \tag{2.10}$$

The local equilibrium hypothesis states that the flow is in constant spectral equilibrium. As a result, energy does not accumulate at any frequency and the shape of the energy spectrum remains invariant in time. As a result, the production, dissipation and energy flux through the cutoff are equal [4, p. 86]:

$$\langle \varepsilon_I \rangle = \langle \tilde{\varepsilon} \rangle = \langle \varepsilon \rangle. \tag{2.11}$$

Using the last equation, we can insert Eq. (2.10) into Eq. (2.8) and get:

$$\begin{aligned}\langle \nu_r \rangle &= \frac{A}{\pi^{4/3}K}\langle \tilde{\varepsilon} \rangle^{\frac{1}{3}} \Delta^{\frac{4}{3}} \\ &= \frac{A}{\pi^{4/3}K}\langle \varepsilon \rangle^{\frac{1}{3}} \Delta^{\frac{4}{3}} \\ &= \frac{A}{\pi^{4/3}K}\left(\frac{1}{\pi^2}\left(\frac{3K}{2}\right)^{-\frac{3}{2}} \Delta^2 \langle 2\overline{S}_{lk}\overline{S}_{lk}\rangle^{\frac{3}{2}}\right)^{\frac{1}{3}} \Delta^{\frac{4}{3}} \\ &= \frac{A}{\pi^2 K}\left(\frac{3K}{2}\right)^{-\frac{1}{2}} \Delta^2 \langle 2\overline{S}_{lk}\overline{S}_{lk}\rangle^{\frac{1}{2}}.\end{aligned}$$

Defining the Smagorinsky coefficient as

$$C_S := \frac{\sqrt{A}}{\pi\sqrt{K}}\left(\frac{3K}{2}\right)^{-\frac{1}{4}} \approx 0.148, \tag{2.12}$$

we can write

$$\langle \nu_r \rangle = (C_S\Delta)^2 \langle 2\overline{S}_{lk}\overline{S}_{lk}\rangle^{\frac{1}{2}}. \tag{2.13}$$

The Smagorinsky model is then expressed as

$$\nu_r(\mathbf{x},t) = (C_S\Delta)^2 \left(2\,\overline{S}_{ij}(\mathbf{x},t)\,\overline{S}_{ij}(\mathbf{x},t)\right)^{\frac{1}{2}}. \tag{2.14}$$

Sagaut admits that there is no particular justification for this except that it is true on average as seen in Eq. (2.13) [4, p. 95]. The model is vindicated by its performance; at least Pope calls it satisfactory, but points out poor performances in certain situations [1, pp. 601ff.].

The Smagorinsky coefficient
The Smagorinsky coefficient C_S was evaluated in Eq. (2.12) but is adjusted to improve results. Through different analyses, the values 0.17 [1, p. 588], [7, p. 76], 0.18 [4, p. 86] and 0.15 [1, p. 590] were obtained as well. The constant is typically between 0.1 and 0.2 [4, p. 95]. It might even be better if C_S is a function of space and time instead of a constant. See Section 2.4 for more details.

2.4 The dynamic Smagorinsky model

It was proposed by Germano et al. [12] (as cited in [6, p. 49]) to view the Smagorinsky coefficient as a function of space and time (c.f. paragraph on p. 7). Lilly [13] developed a form of this idea that is presented here.

Using a so-called test filter $\widehat{\Delta} > \Delta$, the filtered NSE (Eqs. (2.1) and (2.2)) are filtered again:

$$\begin{aligned} \partial_t \widehat{\overline{u}}_j + \partial_i(\widehat{\overline{u}_i \overline{u}_j}) &= \partial_i \left(2\nu \widehat{\overline{S}}_{ij} - \widehat{\tau^r_{ij}}\right) - \partial_j \widehat{\overline{p}} + \widehat{\overline{f}}_j, \quad j = 1,2,3, \quad \text{in } \Omega \times (0,T], \\ \partial_j \widehat{\overline{u}}_j &= 0, \qquad \text{in } \Omega \times [0,T], \end{aligned}$$

with hats denoting the second filtering (see also Eq. (5.5)).
Just as the residual-stress tensor τ^R_{ij} is defined as

$$\tau^R_{ij} := \overline{u_i u_j} - \overline{u}_i \overline{u}_j$$

(see Eq. (5.1)), the subtest-scale stress tensor $\mathbb{K}_{ij}$ is defined as

$$\mathbb{K}_{ij} = \widehat{\overline{u_i u_j}} - \widehat{\overline{u}}_i \widehat{\overline{u}}_j, \tag{2.15}$$

such that

$$\mathbb{L}_{ij} := \mathbb{K}_{ij} - \widehat{\tau^R_{ij}} = \widehat{\overline{u}_i \overline{u}_j} - \widehat{\overline{u}}_i \widehat{\overline{u}}_j. \tag{2.16}$$

$\mathbb{L}_{ij}$ is called the Germano identity [14]. We denote the Smagorinsky parameter with $\widetilde{C}_S$ (instead of C_S). It is written in the ansatz without an exponent, unlike the Smagorinsky coefficient in the Smagorinsky model (Eq. (2.5)). The ansatz is (c.f. Eqs. (2.4) and (2.5)):

$$\begin{aligned} \tau^r_{ij} := \tau^R_{ij} - \frac{1}{3}\tau^R_{kk}\delta_{ij} &= -2\widetilde{C}_S(\mathbf{x},t)\Delta^2 \left(2\overline{S}_{lk}\overline{S}_{lk}\right)^{\frac{1}{2}} \overline{S}_{ij}, \\ \mathbb{K}_{ij} - \frac{1}{3}\mathbb{K}_{kk}\delta_{ij} &= -2\widetilde{C}_S(\mathbf{x},t)\widehat{\Delta}^2 \left(2\widehat{\overline{S}}_{lk}\widehat{\overline{S}}_{lk}\right)^{\frac{1}{2}} \widehat{\overline{S}}_{ij}. \end{aligned}$$

In order to obtain an equation for $\widetilde{C}_S(\mathbf{x},t)$, it is necessary to approximate

$$\widehat{\tau^r_{ij}} \approx -2\widetilde{C}_S(\mathbf{x},t)\Delta^2 \Big[\widehat{\left(2\overline{S}_{lk}\overline{S}_{lk}\right)^{\frac{1}{2}}} \overline{S}_{ij} \Big]. \tag{2.17}$$

We have equality, if the Smagorinsky parameter is independent of $\mathbf{x}$ [6, p. 50]. For $i,j \in \{1,2,3\}$, the system

$$\begin{aligned} \mathbb{L}_{ij} - \frac{1}{3}\mathbb{L}_{kk}\delta_{ij} &= \mathbb{K}_{ij} - \frac{1}{3}\mathbb{K}_{kk}\delta_{ij} - \widehat{\tau^r_{ij}} \\ &\approx -2\widetilde{C}_S \left(\widehat{\Delta}^2 \left(2\widehat{\overline{S}}_{lk}\widehat{\overline{S}}_{lk}\right)^{\frac{1}{2}} \widehat{\overline{S}}_{ij} - \Delta^2 \widehat{\left(2\overline{S}_{lk}\overline{S}_{lk}\right)^{\frac{1}{2}}} \overline{S}_{ij} \right) \\ &= -2\widetilde{C}_S \mathbb{M}_{ij} \end{aligned}$$

with

$$\mathbb{M}_{ij} := \widehat{\Delta}^2 \left(2\widehat{\overline{S}}_{lk}\widehat{\overline{S}}_{lk}\right)^{\frac{1}{2}} \widehat{\overline{S}}_{ij} - \Delta^2 \widehat{\left(2\overline{S}_{lk}\overline{S}_{lk}\right)^{\frac{1}{2}}} \overline{S}_{ij}$$

is an over-determined system which $\widetilde{C}_S$ cannot satisfy exactly [13, p. 633]. Lilly therefore proposes a least-square method minimizing the square of the error

$$Q = \left(\mathbb{L}_{ij} - \frac{1}{3}\mathbb{L}_{kk}\delta_{ij} + 2\widetilde{C}_S\mathbb{M}_{ij} \right)^2,$$

meaning the sum over all i, j. Since

$$\begin{aligned}
\frac{\partial Q}{\partial \widetilde{C}_S} &= 2\left(\mathbb{L}_{ij} - \frac{1}{3}\mathbb{L}_{kk}\delta_{ij} + 2\widetilde{C}_S\mathbb{M}_{ij} \right) 2\mathbb{M}_{ij} \\
&= 4\mathbb{L}_{ij}\mathbb{M}_{ij} - \frac{4}{3}\mathbb{L}_{kk}\delta_{ij}\mathbb{M}_{ij} + 8\widetilde{C}_S\mathbb{M}_{ij}\mathbb{M}_{ij} \\
&= 4\mathbb{L}_{ij}\mathbb{M}_{ij} - \frac{4}{3}\mathbb{L}_{kk}\mathbb{M}_{ll} + 8\widetilde{C}_S\mathbb{M}_{ij}\mathbb{M}_{ij} \\
&= 4\mathbb{L}_{ij}\mathbb{M}_{ij} + 8\widetilde{C}_S\mathbb{M}_{ij}\mathbb{M}_{ij}, \\
\frac{\partial^2 Q}{\partial \widetilde{C}_S^2} &= 8\mathbb{M}_{ij}\mathbb{M}_{ij} > 0,
\end{aligned}$$

the Smagorinsky parameter minimizes the error if we set

$$\widetilde{C}_S(\mathbf{x}, t) = -\frac{\mathbb{L}_{ij}\mathbb{M}_{ij}}{2\mathbb{M}_{ij}\mathbb{M}_{ij}}(\mathbf{x}, t) \tag{2.18}$$

[14, p. 1286]. (Note that $\mathbb{M}_{ll} = 0$ because $\widehat{\overline{S}}_{ll} = 0$ and $\overline{S}_{ll} = 0$, see Eq. (2.2).) Now the twice filtered NSE can be be rewritten analogous to Section 5.A and the model can be applied.
Since the Smagorinsky parameter is not squared like the Smagorinsky coefficient in the Smagorinsky model (Eq. (2.14)), this remark from [6, p. 51] is especially interesting:

> The dynamic subgrid scale model can predict negative values for $\widetilde{C}_S(\mathbf{x}, t)$. This is an advantage since the model allows thus backscatter of energy, in contrast to the Smagorinsky model. However, numerical tests show that $\widetilde{C}_S(\mathbf{x}, t)$ can vary strongly in space and may contain negative values with a very large amplitude. These two properties may strongly destabilize the numerical solution process. In practice, the nominator and denominator of (2.18) are averaged, often in time, to compute a smoother function $\widetilde{C}_S(\mathbf{x}, t)$, e.g., see Lesieur [15, p. 405], Breuer [14] or Sagaut [4, Sect. 4.3.3].[4]

[4] The literature references, equation reference and the variable name in the quote were adjusted to reflect this thesis' reference list and nomenclature.

2.5 Mathematical formulation of the Smagorinsky model

For a mathematical analysis of the Smagorinsky model, we need the problem to be well defined. The vector spaces are defined in the Appendix (see Section 5.B).

2.5.1 Strong and weak formulation of the problem

Consider the NSE with the conditions

$$\begin{aligned} \partial_t \mathbf{u} + (\mathbf{u}\cdot\nabla)\mathbf{u} = \nu\nabla\cdot\nabla\mathbf{u} - \frac{1}{\rho}\nabla P + \mathbf{f} \quad & \text{in } \Omega\times(0,T], \\ \nabla\cdot\mathbf{u} = 0 \quad & \text{in } \Omega\times[0,T], \\ \mathbf{u}(\mathbf{x},0) = \mathbf{u}_0(\mathbf{x}) \quad & \text{in } \Omega, \\ \mathbf{u} = \mathbf{0} \quad & \text{on } \Gamma\times[0,T], \\ \int_\Omega P\,d\mathbf{x} = 0 \quad & \text{in } (0,T]. \end{aligned} \tag{2.19}$$

with $\Gamma = \partial\Omega$. Note that

$$\begin{aligned} 2\partial_i S_{ij} &= \partial_i(\partial_i u_j + \partial_j u_i) = \partial_i\partial_i u_j + \partial_i\partial_j u_i \\ &= \partial_i\partial_i u_j + \partial_j(\partial_i u_i) = \partial_i\partial_i u_j = \nabla\cdot\nabla\mathbf{u}. \end{aligned}$$

The first and second equations are the momentum equation (Eq. (1.2)) and continuity equation (Eq. (1.3)) from above. The initial flow field $\mathbf{u}_0(\mathbf{x})$ is also divergence-free, i.e. $\nabla\cdot\mathbf{u}_0 = 0$ in Ω. The fourth equation is the no slip boundary condition. It is based on the assumption that the fluid neither penetrates nor slips along the wall. Without the last equation, the pressure P would only be determined up to a constant (cf. [2, p. 17]).
Filtering Eqs. (2.19) and using a similar condition for the modified filtered pressure, we get

$$\begin{aligned} \partial_t \overline{\mathbf{u}} + (\overline{\mathbf{u}}\cdot\nabla)\overline{\mathbf{u}} = \nabla\cdot(\nu+\nu_r)\nabla\overline{\mathbf{u}} - \nabla\bar{p} + \overline{\mathbf{f}} \quad & \text{in } \Omega\times(0,T], \\ \nabla\cdot\overline{\mathbf{u}} = 0 \quad & \text{in } \Omega\times[0,T], \\ \overline{\mathbf{u}}(\mathbf{x},0) = \overline{\mathbf{u}}_0(\mathbf{x}) \quad & \text{in } \Omega, \\ \overline{\mathbf{u}} = \mathbf{0} \quad & \text{on } \Gamma\times[0,T], \\ \int_\Omega \bar{p}\,d\mathbf{x} = 0 \quad & \text{in } (0,T]. \end{aligned} \tag{2.20}$$

By multiplying the first equation with $\mathbf{v}\in V$ and integrating over time and space, we achieve a weak formulation:
Let $\overline{\mathbf{f}}\in L^2(0,T;L^2(\Omega))$. Find $\overline{\mathbf{u}}\in V$ that satisfies $\overline{\mathbf{u}}(0,\mathbf{x}) = \overline{\mathbf{u}}_0 \in W^{1,3}_{0,div}(\Omega)$ and

$$\int_0^T (\partial_t\overline{\mathbf{u}} + (\overline{\mathbf{u}}\cdot\nabla)\overline{\mathbf{u}}, \mathbf{v}) + ((\nu+\nu_r)\nabla\overline{\mathbf{u}}, \nabla\mathbf{v})\,dt = \int_0^T (\overline{\mathbf{f}}, \mathbf{v})\,dt \tag{2.21}$$

for all $\mathbf{v} \in V$, with $(\cdot,\cdot)$ denoting the $L^2(\Omega)$ scalar product. Let $\mathbf{n}$ be the outward unit surface normal to $\Gamma = \partial\Omega$. Note that by using integration by parts, we can derive

$$\begin{aligned}(\nabla \cdot \mathbf{w}, \mathbf{v}) &= \int_\Omega (\nabla \cdot \mathbf{w}) \cdot \mathbf{v}\, d\mathbf{x} = \int_\Gamma (\mathbf{w} \cdot \mathbf{n}) \cdot \mathbf{v}\, ds - \int_\Omega \mathbf{w} \cdot (\nabla \mathbf{v})\, d\mathbf{x} \\ &= -\int_\Omega \mathbf{w} \cdot (\nabla \mathbf{v})\, d\mathbf{x} = -(\mathbf{w}, \nabla \mathbf{v}),\end{aligned}$$

because $\mathbf{v} = \mathbf{0}$ on Γ. In this case, we used $\mathbf{w} = (\nu + \nu_r)\nabla\overline{\mathbf{u}}$. The pressure term vanishes because

$$(\nabla \bar{p}, \mathbf{v}) = \int_\Omega \nabla \bar{p} \cdot \mathbf{v}\, d\mathbf{x} = \int_\Gamma \bar{p}\,(\mathbf{v} \cdot \mathbf{n})\, ds - \int_\Omega \bar{p}\,(\nabla \cdot \mathbf{v})\, d\mathbf{x} = 0,$$

as $\nabla \cdot \mathbf{v} = 0$.
Another similar variation of this formulation is:
Find $(\mathbf{w}, q) : [0,T] \to X \times Q$ satisfying $\mathbf{w}(\mathbf{x}, 0) = \overline{\mathbf{u}}_0(\mathbf{x})$ and

$$(\partial_t \mathbf{w}, \mathbf{v}) + a(\mathbf{w}, \mathbf{w}, \mathbf{v}) + b(\mathbf{w}, \mathbf{w}, \mathbf{v}) + (\lambda, \nabla \cdot \mathbf{w}) - (q, \nabla \cdot \mathbf{v}) = (\overline{\mathbf{f}}, \mathbf{v}) \quad (2.22)$$

for all $(\mathbf{v}, \lambda) \in X \times Q$ with

$$\begin{aligned}a(\mathbf{u}, \mathbf{w}, \mathbf{v}) &:= \alpha(\nabla \cdot \mathbf{w}, \nabla \cdot \mathbf{v}) \\ &\quad + \left(\left(2\mathrm{Re}^{-1} + \widetilde{C}_S \Delta^2 \left(\overline{S}_{lk}(\mathbf{u})\overline{S}_{lk}(\mathbf{u})\right)^{\frac{1}{2}}\right)\overline{S}(\mathbf{w}), \overline{S}(\mathbf{v})\right) \\ b(\mathbf{u}, \mathbf{w}, \mathbf{v}) &:= \frac{1}{2}(\mathbf{u} \cdot \nabla \mathbf{w}, \mathbf{v}) - \frac{1}{2}(\mathbf{u} \cdot \nabla \mathbf{v}, \mathbf{w})\end{aligned}$$

(with the Smagorinsky parameter $\widetilde{C}_S = \sqrt{2}C_S^2$) [5, p. 1002].

2.6 Existence and uniqueness of solutions

It has been shown by Ladyzhenskaya [16], [17] (see also [6, pp. 74ff.]) that the Smagorinsky model has a unique and stable solution under certain conditions. She considers the Smagorinsky model with no slip boundary conditions (Eqs. (2.20)) and derives the weak formulation of the problem (Eqs. (2.21)).
Ladyzhenskaya then proves the solvability of this equation with the Galerkin method: A sequence of functions in V is constructed that solves finite-dimensional approximations of the equation. If $\overline{\mathbf{f}} \in L^2\left(0, T; L^2(\Omega)\right)$ and $\overline{\mathbf{u}}_0 \in W^{1,3}_{0,div}(\Omega)$, a subsequence converges to a solution $\overline{\mathbf{u}} \in V$ of the equation that is also unique and stable.

2.7 Numerical analysis of the Smagorinsky model

John and Layton [5] provide an analytic approach to error estimates in LES. They consider the NSE with initial and no-slip boundary conditions (Eqs. (2.19)). (To be precise, they use slip with linear friction, but the formulas can be interpreted to mean no-slip condition as well.) After applying the filter, the resulting system is (2.20). For simplicity, the inflow velocity is set to zero.
The following problem is discussed:
Find solutions $(\mathbf{w}, q) \in X \times Q$ (see Eqs. (5.10) and (5.11)) that approximate $(\overline{\mathbf{u}}, \bar{p})$. The properties of $(\overline{\mathbf{u}}, \bar{p})$ (e.g. smoothness) do not necessarily have to apply to the approximations $(\mathbf{w}, q)$ [5, p. 998].
The solution is approximated with a finite element method. For the representative mesh width h, the respective solution for a variational problem (Eq. (2.22)) is $(\mathbf{w}^h, q^h) \in X^h \times Q^h$ with appropriate finite element spaces $X^h \subset X$ and $Q^h \times Q$. Du and Gunzburger have proven that the discrete solutions converge to the solution of the continuous problem under minimal regularity assumption on the solution [18] (as cited in [6, p. 126]).
In order for the Smagorinsky term to be well defined, the natural regularity of the weak solution of the Smagorinsky model is

$$\nabla \mathbf{w} \in L^3(0, T; L^3(\Omega)) \tag{2.23}$$

[6, p. 136]. As mentioned in Section 2.6, the solution is unique.
John and Layton's [5] (see also [6, pp. 126-158]) error estimate analysis does not work if the only assumption is (2.23). However, they do find a ν-independent error estimate, if the residual subgrid-scale eddy viscosity $\nu_r(\Delta, \mathbf{w})$ has another term $a_0(\Delta) > 0$ [6, p. 136].
Alternatively, for $a_0(\Delta) = 0$, the assumption

$$\nabla \mathbf{w} \in L^2(0, T; L^\infty(\Omega))$$

is needed for such an error estimate [6, pp. 149-152].

3 Numerical Studies

3.1 The benchmark problem: surface mounted cube

We consider the benchmark problem of flow of an incompressible Newtonian fluid around a surface mounted cube, examined by Hoffmann and Johnson [3, pp. 12ff.] and others [19], [20]. Hoffman and Johnson [3, p. 12] describe the channel and cube as follows:

> The cube side length is $H = 0.1$, and the cube is centrally mounted on the floor of a rectangular channel of length $15H$, height $2H$, and width $7H$, at a distance of $3.5H$ from the inlet.

Figures 1 to 3 illustrate this. These figures also show the pressure building up in front of the cube.

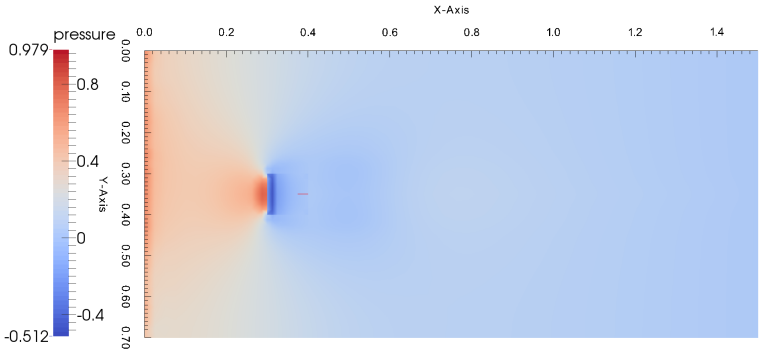

Figure 1: View from below the channel.

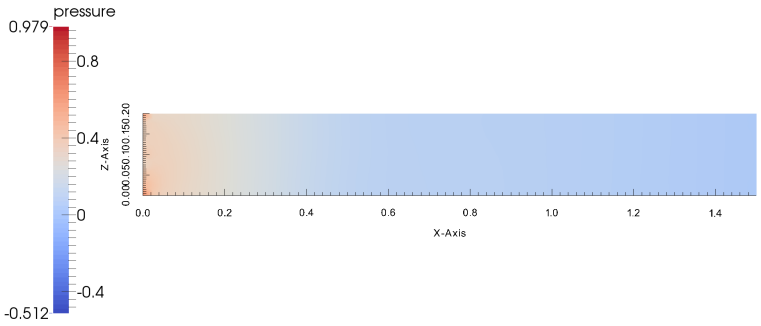

Figure 2: View of the side of the channel.

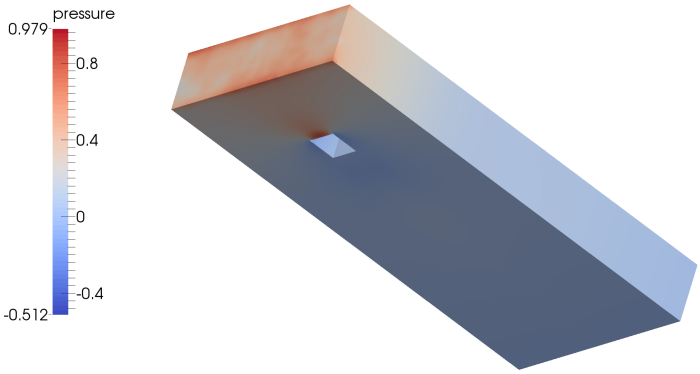

Figure 3: View from an angle.

We choose the characteristic velocity, characteristic length and kinetic viscosity

$$U = 1\,\frac{\mathrm{m}}{\mathrm{s}}, \qquad L = H = 0.1\,\mathrm{m}, \qquad \nu = 2.5 \cdot 10^{-6}\,\frac{\mathrm{m}^2}{\mathrm{s}},$$

such that the Reynolds number equals

$$\mathrm{Re} = \frac{UL}{\nu} = \frac{1\,\frac{\mathrm{m}}{\mathrm{s}} \cdot 0.1\,\mathrm{m}}{2.5 \cdot 10^{-6}\,\frac{\mathrm{m}^2}{\mathrm{s}}} = 40\,000.$$

Hoffman [19, pp. 191f.] describes further conditions:

> The inlet velocity profile is interpolated from experiments, and we use no slip boundary conditions on the cube and the vertical channel boundaries, slip boundary conditions on the lateral channel boundaries, and a transparent outflow boundary condition.

The mean inlet velocity is 1, the same as the characteristic velocity U. See Section 5.C for more information.
We are interested in the drag and lift coefficients corresponding to the drag and lift force on the cube, which is discussed in Section 3.2.

3.1.1 Implementation of the Smagorinsky model

Using finite elements, the Smagorinsky model was implemented in its weak form (Eq. (2.22)) with the code MooNMD (see also [21]). The grid was uniformly refined 3 or 4 times; thus we call them level 3 or level 4 simulations. The degrees of freedom of velocity and pressure for both simulation types are shown in Table 1.
The turbulent viscosity constant

$$\nu_{\mathrm{turb}} = \widetilde{C}_S \Delta^2 \tag{3.1}$$

	velocity	pressure
level 3	134 739	20 224
level 4	1 023 651	161 792

Table 1: The degrees of freedom of velocity and pressure.

was chosen between 0.005 and 0.1. The filter width Δ is the shortest edge. Five seconds of the flow was simulated, with time step lengths 0.005, 0.01 or 0.02.
Figures 1 to 5 show how the pressure is distributed. In this particular simulation, the turbulent viscosity constant was $\nu_{\text{turb}} = 0.055$, the time step length was 0.005 and the grid was refined 4 times. The last time frame was chosen. As was to be expected, pressure builds up in front of the cube. This pressure plays an important part in the drag and lift forces on the cube.

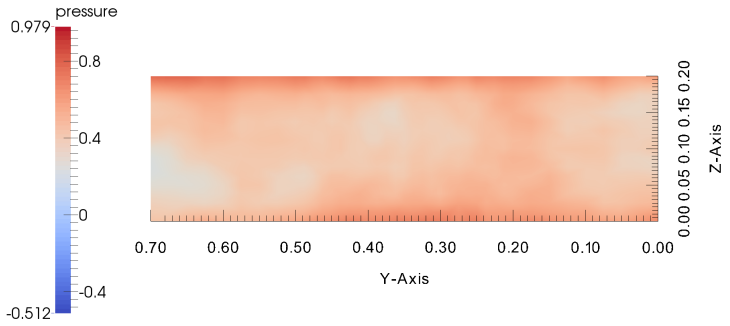

Figure 4: View of the front of the channel.

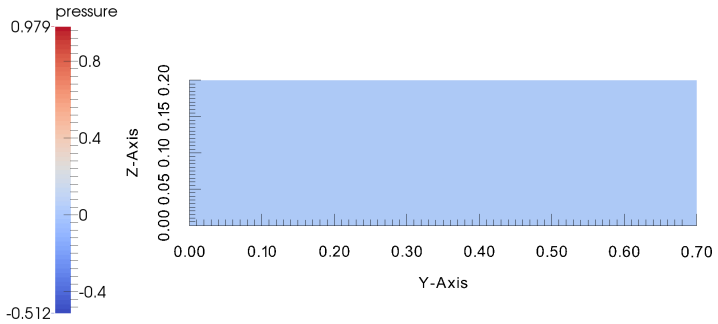

Figure 5: View of the back of the channel.

3.2 Lift and drag

There are two ways to calculate the drag and lift coefficients: using area integrals and using volume integrals. In the literature, the drag and lift coefficients are defined as area integrals. Therefore, the first method is presented in Section 3.2.3. The second method was used in the simulations we present here, as it is known to perform better numerically. It is presented in Section 3.2.4.

3.2.1 Lift and drag forces

The drag and lift force on a body such as the cube is given by

$$\begin{aligned} F_{\mathbf{w}} &= -\int_{\Gamma_{\text{cube}}} \mathbb{S}_{ij} n_j w_i \, ds = -\int_{\Gamma_{\text{cube}}} (2\mu S_{ij} - P\delta_{ij}) \, n_j w_i \, ds \\ &= -\int_{\Gamma_{\text{cube}}} (\mu(\partial_i u_j + \partial_j u_i) - P\delta_{ij}) \, n_j w_i \, ds \quad [N] \end{aligned}$$

with the stress tensor

$$\mathbb{S}_{ij} = 2\mu S_{ij} - P\delta_{ij} \tag{3.2}$$

and $\mathbf{n} = (n_1, n_2, n_3)^T$ the unit vector which points outward with respect to the flow domain Ω. The unit vector $\mathbf{w}$ points in the direction of the flow for the drag force and perpendicular to it for the lift force [3, Eq. (6)].
The dimensionless version is

$$\begin{aligned} F_{\mathbf{w}} &= -L^2 \int_{\Gamma_{\text{cube}}} \left(\frac{\mu U}{L} (\partial_i v_j + \partial_j v_i) - \rho U^2 \hat{p} \delta_{ij} \right) n_j w_i \, ds \\ &= -\rho U^2 L^2 \int_{\Gamma_{\text{cube}}} \left(\frac{\mu}{\rho U L} (\partial_i v_j + \partial_j v_i) - \hat{p} \delta_{ij} \right) n_j w_i \, ds \\ &= -\rho U^2 L^2 \int_{\Gamma_{\text{cube}}} \left(\mathrm{Re}^{-1} (\partial_i v_j + \partial_j v_i) - \hat{p} \delta_{ij} \right) n_j w_i \, ds \end{aligned} \tag{3.3}$$

with the characteristic length L, characteristic velocity U, dimensionless velocity $v_i = u_i/U$ and dimensionless pressure

$$\hat{p} = \frac{P}{\rho U^2} \, . \tag{3.4}$$

In the first line, the factor L^2 before the integral comes from the transform of the integral and the factor $1/L$ in the integral comes from the transformation of the spatial derivatives.
With $\mathbf{w} = (1, 0, 0)^T$ or $\mathbf{w} = (0, 1, 0)^T$ respectively, we now have:

$$F_{\text{drag}} = -\rho U^2 L^2 \int_{\Gamma_{\text{cube}}} \left(\mathrm{Re}^{-1} (\partial_1 v_j + \partial_j v_1) - \hat{p} \delta_{1j} \right) n_j \, ds, \tag{3.5}$$

$$F_{\text{lift}} = -\rho U^2 L^2 \int_{\Gamma_{\text{cube}}} \left(\mathrm{Re}^{-1} (\partial_2 v_j + \partial_j v_2) - \hat{p} \delta_{2j} \right) n_j \, ds. \tag{3.6}$$

3.2.2 Simplifying the equations for a wall-mounted cube

Since $\mathbf{u} = \mathbf{0}$ on the cube surface Γ_{cube}, tangential derivatives vanish. We will split the integral into 5 parts, one for each side.
Let $\Gamma_{\text{cube}} = \Gamma_1 \cup \Gamma_2 \cup \Gamma_3$ with intersections of different Γ_i having zero area. Let Γ_1 be the two sides of the cube where the unit normal vector only takes the values $\mathbf{n} = (\pm 1, 0, 0)^T$ (front and back side), Γ_2 the two sides where the unit normal vector only takes the values $\mathbf{n} = (0, \pm 1, 0)^T$ (right and left side) and Γ_3 the top side, i.e. the unit normal vector only takes the value $\mathbf{n} = (0, 0, -1)^T$.
To use a simple notation, we write

$$\int_{\Gamma_1} \pm 2\text{Re}^{-1}\partial_1 v_1 \mp \hat{p}\, ds,$$

when we mean $\int_{\Gamma_1} 2\text{Re}^{-1}\partial_1 v_1 - \hat{p}\, ds$ evaluated on the back side of the cube plus $\int_{\Gamma_1} -2\text{Re}^{-1}\partial_1 v_1 + \hat{p}\, ds$ evaluated on the front side.
Then the forces are

$$\begin{aligned} F_{\text{drag}} = -\rho U^2 L^2 \Bigg(&\int_{\Gamma_1} \pm 2\text{Re}^{-1}\partial_1 v_1 \mp \hat{p}\, ds + \int_{\Gamma_2} \pm \text{Re}^{-1}(\partial_1 v_2 + \partial_2 v_1)\, ds \\ &- \int_{\Gamma_3} \text{Re}^{-1}(\partial_1 v_3 + \partial_3 v_1)\, ds \Bigg), \\ F_{\text{lift}} = -\rho U^2 L^2 \Bigg(&\int_{\Gamma_1} \pm \text{Re}^{-1}(\partial_2 v_1 + \partial_1 v_2)\, ds + \int_{\Gamma_2} \pm 2\text{Re}^{-1}\partial_2 v_2 \mp \hat{p}\, ds \\ &- \int_{\Gamma_3} \text{Re}^{-1}(\partial_2 v_3 + \partial_3 v_2)\, ds \Bigg). \end{aligned}$$

Taking into account that the tangential derivatives vanish:

$$\begin{aligned} \nabla v_i \cdot (1,0,0)^T = \partial_1 v_i = 0 \quad &\text{for } \Gamma_2, \Gamma_3,\ i = 1,2,3, \\ \nabla v_i \cdot (0,1,0)^T = \partial_2 v_i = 0 \quad &\text{for } \Gamma_1, \Gamma_3,\ i = 1,2,3, \\ \nabla v_i \cdot (0,0,1)^T = \partial_3 v_i = 0 \quad &\text{for } \Gamma_1, \Gamma_2,\ i = 1,2,3, \end{aligned}$$

the equations simplify to

$$\begin{aligned} F_{\text{drag}} = -\rho U^2 L^2 \Bigg(&\int_{\Gamma_1} \pm 2\text{Re}^{-1}\partial_1 v_1 \mp \hat{p}\, ds + \int_{\Gamma_2} \pm \text{Re}^{-1}\partial_2 v_1\, ds \\ &- \int_{\Gamma_3} \text{Re}^{-1}\partial_3 v_1\, ds \Bigg), \\ F_{\text{lift}} = -\rho U^2 L^2 \Bigg(&\int_{\Gamma_1} \pm \text{Re}^{-1}\partial_1 v_2\, ds + \int_{\Gamma_2} \pm 2\text{Re}^{-1}\partial_2 v_2 \mp \hat{p}\, ds \\ &- \int_{\Gamma_3} \text{Re}^{-1}\partial_3 v_2\, ds \Bigg). \end{aligned}$$

3.2.3 Lift and drag coefficients

The lift and drag equations are

$$c_{\text{drag}} = \frac{2F_{\text{drag}}}{\rho A V^2}, \qquad c_{\text{lift}} = \frac{2F_{\text{lift}}}{\rho A V^2} \tag{3.7}$$

with V being the speed of the fluid and A being the reference area. Here the mean inflow is $V = U = 1\,\frac{\text{m}}{\text{s}}$ and the reference area is one side of the cube $A = H^2 = 0.001\,\text{m}^2$.
The factor in the equations for the drag and lift force is $-\rho U^2 L^2$, the factor for the lift and drag coefficients is therefore

$$-\frac{2\rho U^2 L^2}{\rho A V^2} = -\frac{2U^2 L^2}{AV^2} = -\frac{2U^2 H^2}{H^2 U^2} = -2. \tag{3.8}$$

Finally, the drag and lift coefficients are

$$\begin{aligned}
c_{\text{drag}} &= -2\int_{\Gamma_{\text{cube}}} \left(\text{Re}^{-1}(\partial_1 v_j + \partial_j v_1) - \hat{p}\delta_{1j}\right) n_j \, ds \\
&= -2\left(\int_{\Gamma_1} \pm 2\text{Re}^{-1}\partial_1 v_1 \mp \hat{p}\, ds + \int_{\Gamma_2} \pm \text{Re}^{-1}\partial_2 v_1 \, ds \right. \\
&\quad \left. - \int_{\Gamma_3} \text{Re}^{-1}\partial_3 v_1 \, ds\right), \\
c_{\text{lift}} &= -2\int_{\Gamma_{\text{cube}}} \left(\text{Re}^{-1}(\partial_2 v_j + \partial_j v_2) - \hat{p}\delta_{2j}\right) n_j \, ds \\
&= -2\left(\int_{\Gamma_1} \pm \text{Re}^{-1}\partial_1 v_2 \, ds + \int_{\Gamma_2} \pm 2\text{Re}^{-1}\partial_2 v_2 \mp \hat{p}\, ds \right. \\
&\quad \left. - \int_{\Gamma_3} \text{Re}^{-1}\partial_3 v_2 \, ds\right).
\end{aligned}$$

3.2.4 Alternative calculation for lift and drag

Alternatively, the lift and drag force (and lift and drag coefficients) can be computed using volume integrals. First, we rewrite the dimensionless version of the drag and lift force (Eq. (3.3)) as

$$F_{\mathbf{w}} = -\rho U^2 L^2 \int_{\Gamma_{\text{cube}}} \left(\left(2\text{Re}^{-1} S(\mathbf{v}) - \hat{p}\mathbb{I}\right)\mathbf{n}\right) \cdot \mathbf{w}\, ds. \tag{3.9}$$

We will use the momentum equation to find another expression for the integral. If the cube was not attached to the rest of the boundary, that is $\overline{\Gamma_{\text{cube}}} \cap \overline{\Gamma \backslash \Gamma_{\text{cube}}} = \emptyset$, one could extent $\mathbf{w}$ to a function in Ω such that $\mathbf{w} \in H^1(\Omega)$ and $\mathbf{w}$ vanishes at $\overline{\Gamma \backslash \Gamma_{\text{cube}}}$. In practice, this is done despite the body (such as the cube) being attached to the rest of the boundary [22, p. 848], [23, pp. 6007-6009].

We take the dimensionless version of the momentum equation (Eq. (1.2)):

$$\partial_t \mathbf{v} + (\mathbf{v}\cdot\nabla)\mathbf{v} = 2\mathrm{Re}^{-1}\nabla\cdot S(\mathbf{v}) - \nabla\hat{p} + \mathbf{f}.$$

Here the force $\mathbf{f}$ is dimensionless with abuse of notation and we again assume $\mathbf{f} \in L^2(0,T;L^2(\Omega))$. Testing the equation with $\mathbf{w}$ (analogous to Section 2.5.1) gives the weak form

$$(\partial_t \mathbf{v},\mathbf{w}) + ((\mathbf{v}\cdot\nabla)\mathbf{v},\mathbf{w}) = (2\mathrm{Re}^{-1}\nabla\cdot S(\mathbf{v}),\mathbf{w}) - (\nabla\hat{p},\mathbf{w}) + (\mathbf{f},\mathbf{w}).$$

Using integration by parts, we get

$$\begin{aligned}(\partial_t \mathbf{v},\mathbf{w}) + ((\mathbf{v}\cdot\nabla)\mathbf{v},\mathbf{w}) = \int_\Gamma \left(2\mathrm{Re}^{-1}S(\mathbf{v})\,\mathbf{n}\right)\cdot\mathbf{w}\,ds - (2\mathrm{Re}^{-1}S(\mathbf{v}),\nabla\mathbf{w})\\ - \int_\Gamma \hat{p}\,\mathbf{n}\cdot\mathbf{w}\,ds + (\hat{p},\nabla\cdot\mathbf{w}) + (\mathbf{f},\mathbf{w}).\end{aligned}$$

Since $\mathbf{w}$ vanishes on $\overline{\Gamma\backslash\Gamma_{\mathrm{cube}}}$, this is equivalent to

$$\begin{aligned}(\partial_t \mathbf{v},\mathbf{w}) + ((\mathbf{v}\cdot\nabla)\mathbf{v},\mathbf{w}) + (2\mathrm{Re}^{-1}S(\mathbf{v}),\nabla\mathbf{w}) - (\hat{p},\nabla\cdot\mathbf{w})\\ -(\mathbf{f},\mathbf{w}) = \int_{\Gamma_{\mathrm{cube}}} \left(\left(2\mathrm{Re}^{-1}S(\mathbf{v}) - \hat{p}\mathbb{I}\right)\mathbf{n}\right)\cdot\mathbf{w}\,ds.\end{aligned}$$

We can insert the last equation into Eq. (3.9) such that

$$\begin{aligned}F_{\mathbf{w}} = -\rho U^2 L^2\big[(\partial_t \mathbf{v},\mathbf{w}) + ((\mathbf{v}\cdot\nabla)\mathbf{v},\mathbf{w}) + \left(2\mathrm{Re}^{-1}S(\mathbf{v}),\nabla\mathbf{w}\right)\\ - (\hat{p},\nabla\cdot\mathbf{w}) - (\mathbf{f},\mathbf{w})\big].\end{aligned} \tag{3.10}$$

We want to show

$$(2\mathrm{Re}^{-1}S(\mathbf{v}),\nabla\mathbf{w}) = (2\mathrm{Re}^{-1}S(\mathbf{v}),S(\mathbf{w})).$$

First, we show that

$$\begin{aligned}(2\mathrm{Re}^{-1}S(\mathbf{v}),\nabla\mathbf{w}) &= \int_\Omega 2\mathrm{Re}^{-1}S_{ij}(\mathbf{v})\,\partial_i w_j\,d\mathbf{x}\\ &= \int_\Omega 2\mathrm{Re}^{-1}S_{ji}(\mathbf{v})\,\partial_j w_i\,d\mathbf{x}\\ &= \int_\Omega 2\mathrm{Re}^{-1}S_{ij}(\mathbf{v})\,\partial_j w_i\,d\mathbf{x}\\ &= \left(2\mathrm{Re}^{-1}S(\mathbf{u}),(\nabla\mathbf{w})^T\right).\end{aligned}$$

The rate-of-strain tensor $S(\mathbf{v})$ is symmetric, which can be easily seen from the definition. Finally,

$$\begin{aligned}(2\mathrm{Re}^{-1}S(\mathbf{v}),\nabla\mathbf{w}) &= \left(2\mathrm{Re}^{-1}S(\mathbf{v}),\frac{1}{2}(\nabla\mathbf{w}+\nabla\mathbf{w})\right)\\ &= \left(2\mathrm{Re}^{-1}S(\mathbf{v}),\frac{1}{2}(\nabla\mathbf{w}+(\nabla\mathbf{w})^T)\right)\\ &= (2\mathrm{Re}^{-1}S(\mathbf{v}),S(\mathbf{w})).\end{aligned}$$

Now we can rewrite Eq. (3.10):

$$F_{\mathbf{w}} = -\rho U^2 L^2 \big[(\partial_t \mathbf{v}, \mathbf{w}) + ((\mathbf{v}\cdot\nabla)\mathbf{v}, \mathbf{w}) + \big(2\mathrm{Re}^{-1} S(\mathbf{v}), S(\mathbf{w})\big) - (\hat{p}, \nabla\cdot\mathbf{w}) - (\mathbf{f}, \mathbf{w})\big].$$

Choosing the appropriate $\mathbf{w}$ as in Section 3.2.1, i.e. $\mathbf{w}_{\mathrm{drag}} = (1,0,0)^T$ on Γ_{cube} for drag and $\mathbf{w}_{\mathrm{lift}} = (0,1,0)^T$ on Γ_{cube} for lift, we get the drag and lift forces

$$\begin{aligned} F_{\mathrm{drag}} &= -\rho U^2 L^2 \big[(\partial_t \mathbf{v}, \mathbf{w}_{\mathrm{drag}}) + ((\mathbf{v}\cdot\nabla)\mathbf{v}, \mathbf{w}_{\mathrm{drag}}) + \big(2\mathrm{Re}^{-1} S(\mathbf{v}), S(\mathbf{w}_{\mathrm{drag}})\big) \\ &\qquad - (\hat{p}, \nabla\cdot\mathbf{w}_{\mathrm{drag}}) - (\mathbf{f}, \mathbf{w}_{\mathrm{drag}})\big], \\ F_{\mathrm{lift}} &= -\rho U^2 L^2 \big[(\partial_t \mathbf{v}, \mathbf{w}_{\mathrm{drag}}) + ((\mathbf{v}\cdot\nabla)\mathbf{v}, \mathbf{w}_{\mathrm{drag}}) + \big(2\mathrm{Re}^{-1} S(\mathbf{v}), S(\mathbf{w}_{\mathrm{drag}})\big) \\ &\qquad - (\hat{p}, \nabla\cdot\mathbf{w}_{\mathrm{drag}}) - (\mathbf{f}, \mathbf{w}_{\mathrm{drag}})\big]. \end{aligned}$$

With Eqs. (3.7) and (3.8), the drag and lift coefficients can be computed with

$$\begin{aligned} c_{\mathrm{drag}} &= -2\big[(\partial_t \mathbf{v}, \mathbf{w}_{\mathrm{drag}}) + ((\mathbf{v}\cdot\nabla)\mathbf{v}, \mathbf{w}_{\mathrm{drag}}) + \big(2\mathrm{Re}^{-1} S(\mathbf{v}), S(\mathbf{w}_{\mathrm{drag}})\big) \\ &\qquad - (\hat{p}, \nabla\cdot\mathbf{w}_{\mathrm{drag}}) - (\mathbf{f}, \mathbf{w}_{\mathrm{drag}})\big], \qquad (3.11) \\ c_{\mathrm{lift}} &= -2\big[(\partial_t \mathbf{v}, \mathbf{w}_{\mathrm{drag}}) + ((\mathbf{v}\cdot\nabla)\mathbf{v}, \mathbf{w}_{\mathrm{drag}}) + \big(2\mathrm{Re}^{-1} S(\mathbf{v}), S(\mathbf{w}_{\mathrm{drag}})\big) \\ &\qquad - (\hat{p}, \nabla\cdot\mathbf{w}_{\mathrm{drag}}) - (\mathbf{f}, \mathbf{w}_{\mathrm{drag}})\big]. \qquad (3.12) \end{aligned}$$

3.3 Results of numerical simulations

We evaluated the drag and lift coefficients using Eqs. (3.11) and (3.12) and the implementation mentioned above (see Section 3.1.1). The following figures always include the mean value (blue line) and the standard deviation of the data points (blue shade).
The graphs of the lift and drag coefficients (Figures 6 to 12) oscillate, as was to be expected in a turbulent flow. The graph oscillates around the mean value in Figures 6 to 9. However, if the turbulent viscosity constant ν_{turb} is below 0.05, the graph shows a different oscillatory pattern that is different for different time step lengths (Figures 10 to 12).

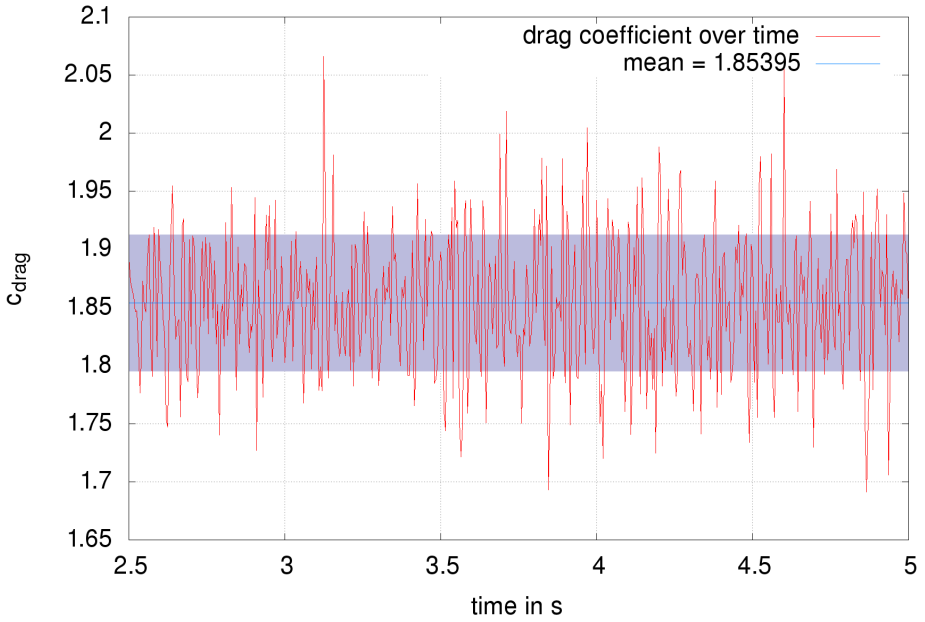

Figure 6: Drag coefficient for a level 3 simulation with turbulent viscosity constant $\nu_{\text{turb}} = 0.055$ and time step length 0.005.

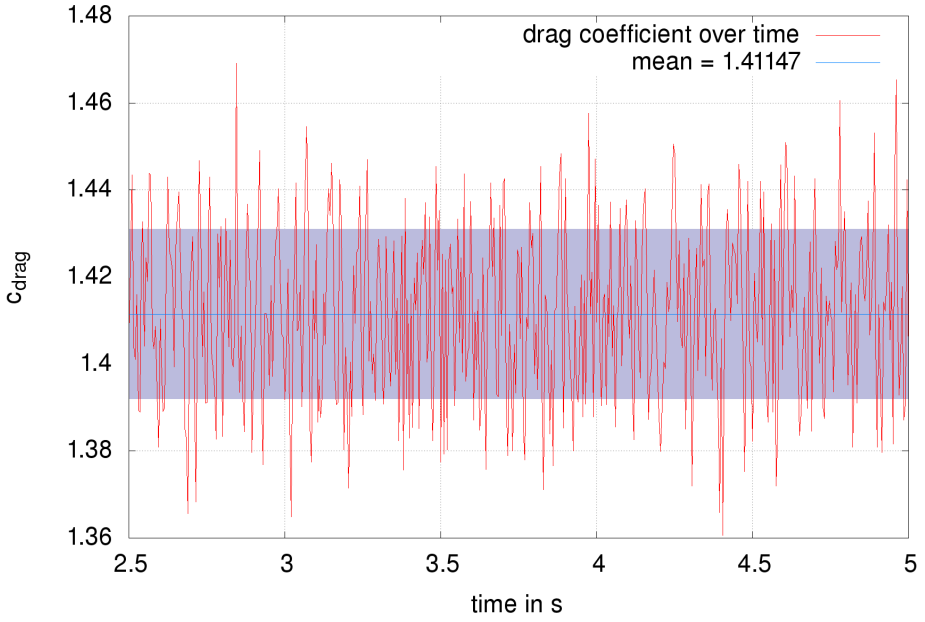

Figure 7: Drag coefficient for a level 4 simulation with turbulent viscosity constant $\nu_{\text{turb}} = 0.055$ and time step length 0.005.

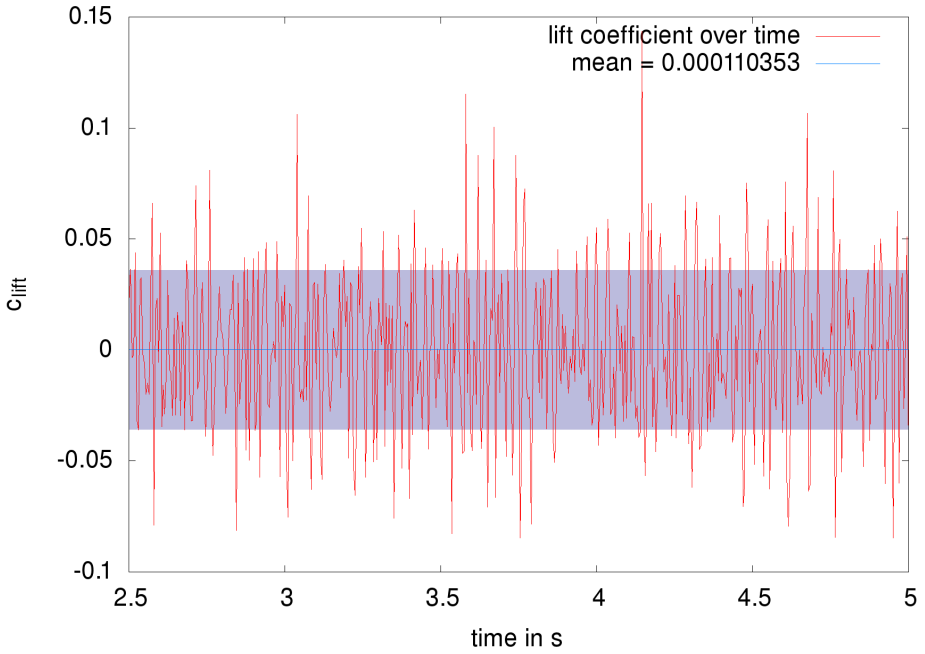

Figure 8: Lift coefficient for a level 3 simulation with turbulent viscosity constant $\nu_{\text{turb}} = 0.055$ and time step length 0.005.

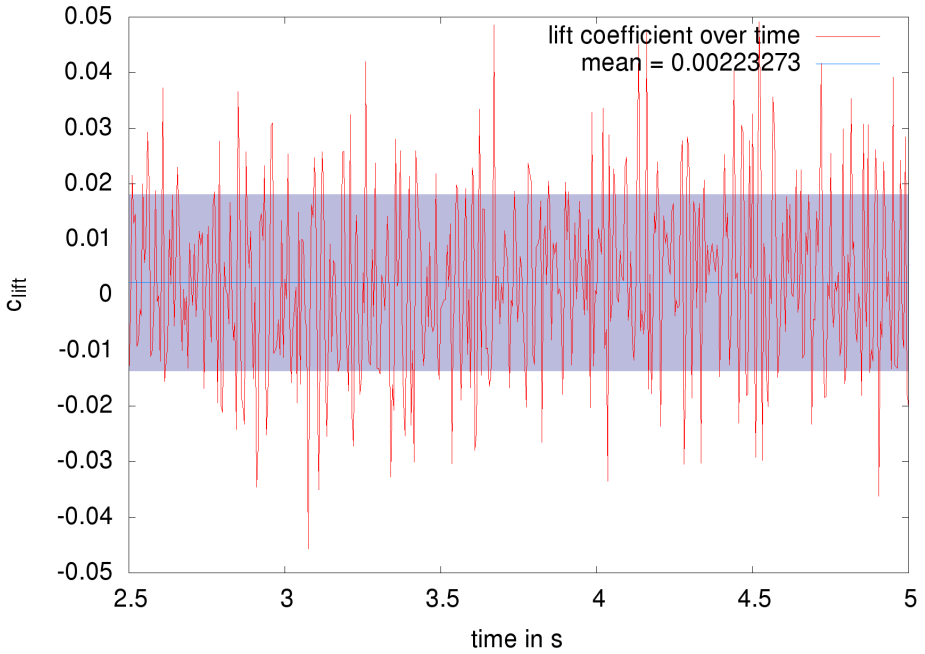

Figure 9: Lift coefficient for a level 4 simulation with turbulent viscosity constant $\nu_{\text{turb}} = 0.055$ and time step length 0.005.

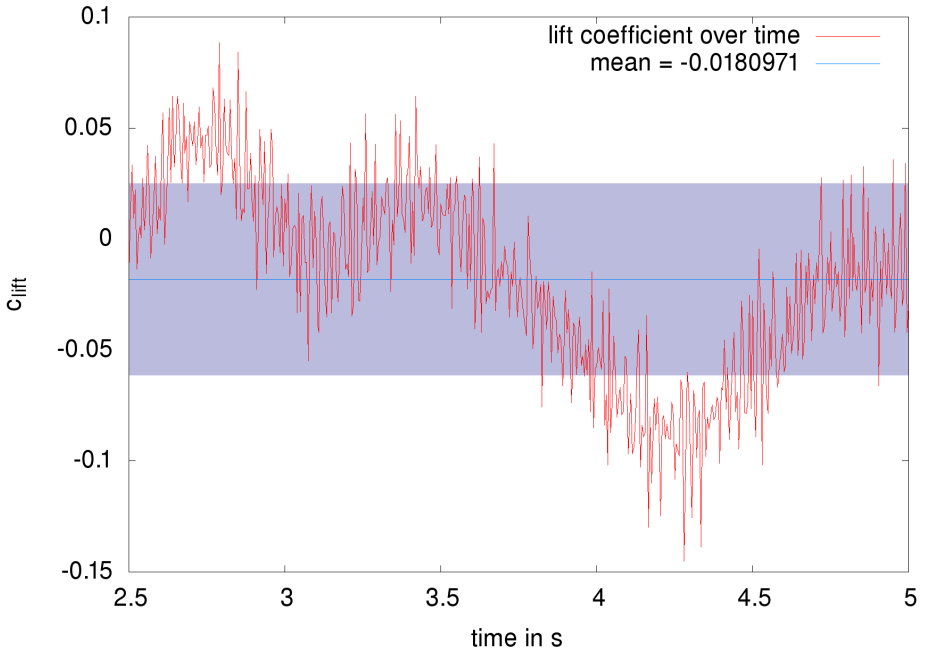

Figure 10: Lift coefficient for a level 4 simulation with turbulent viscosity constant $\nu_{\text{turb}} = 0.005$ and time step length 0.005.

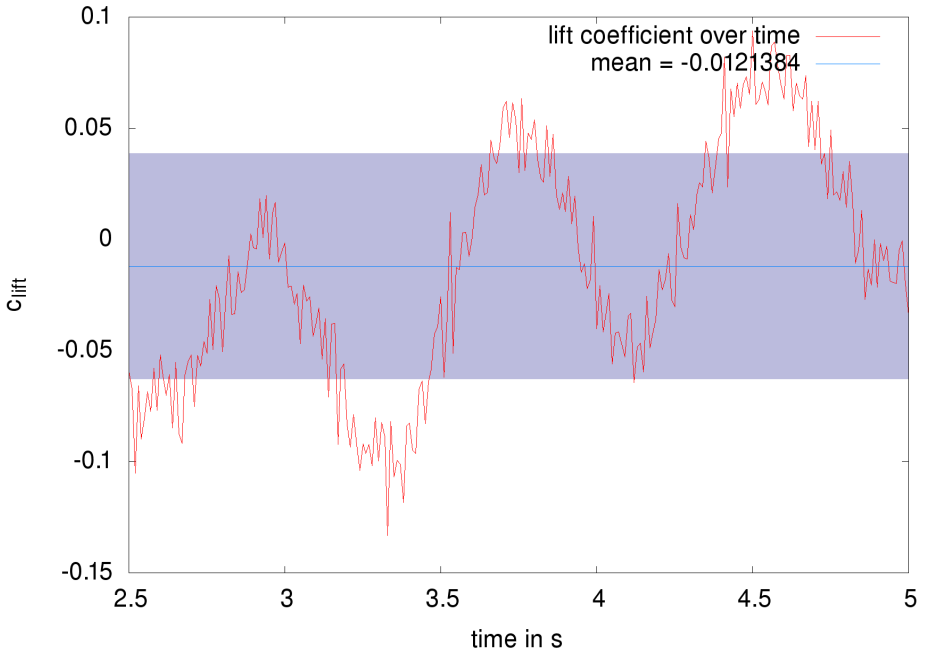

Figure 11: Lift coefficient for a level 4 simulation with turbulent viscosity constant $\nu_{\text{turb}} = 0.005$ and time step length 0.01.

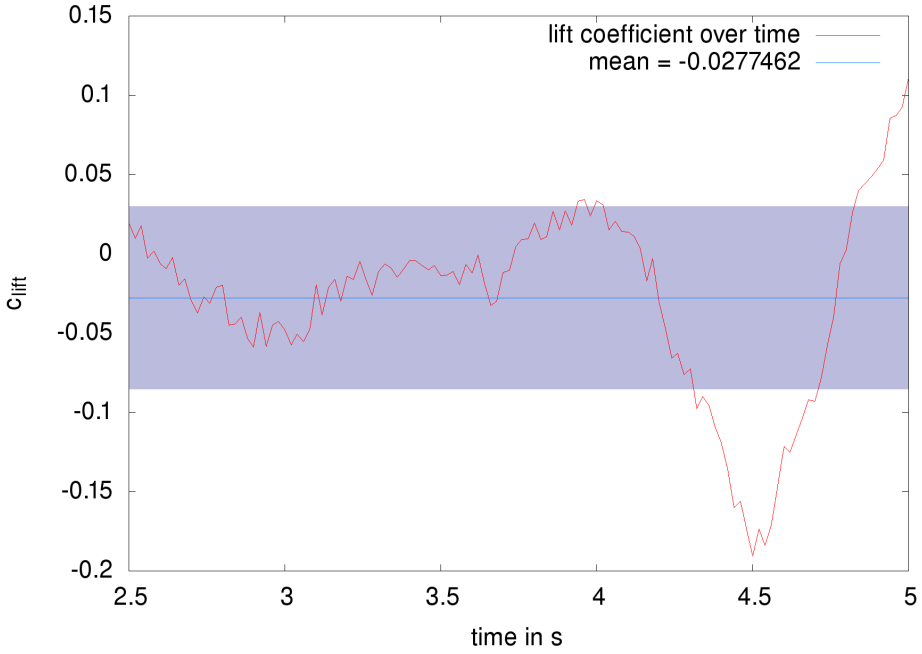

Figure 12: Lift coefficient for a level 4 simulation with turbulent viscosity constant $\nu_{\text{turb}} = 0.005$ and time step length 0.02.

3.3.1 Mean drag coefficient

We calculate the arithmetic mean of the drag coefficients in the time interval $I = [2.5, 5]$, called mean drag coefficient. The mean lift coefficient is not of interest, as it is always about 0 because of symmetry.
The resulting mean drag values of the MooNMD simulations are shown in Tables 2 and 3, which are visualized in Figures 13 and 14, respectively.

Level 3		**time step length**		
		0.005	0.010	0.020
turbulent viscosity constant	0.005	1.16178	1.16146	1.16280
	0.010	1.26270	1.26244	1.26378
	0.015	1.35410	1.35381	1.35505
	0.020	1.44258	1.44225	1.44349
	0.025	1.51808	1.51776	1.51897
	0.030	1.58505	1.58462	1.58580
	0.035	1.64603	1.64557	1.64666
	0.040	1.70253	1.70212	1.70313
	0.045	1.75556	1.75537	1.75615
	0.050	1.80584	1.80554	1.80634
	0.055	1.85395	1.85360	1.85433
	0.060	1.90029	1.89998	1.90072
	0.065	1.94527	1.94490	1.94573
	0.070	1.98923	1.98905	1.98955
	0.075	2.03230	2.03222	2.03257
	0.080	2.07460	2.07440	2.07493
	0.085	2.11644	2.11629	2.11672
	0.090	2.15782	2.15746	2.15803
	0.095	2.19872	2.19843	2.19896
	0.100	2.23937	2.23916	2.23945

Table 2: Mean drag values for level 3 simulations. The data is visualized in Fig. 13.

In level 3 simulations, the differences between mean drag values corresponding to the same turbulent viscosity constant ν_{turb} but different time step lengths are less than 0.0015. That is why in Fig. 13, only one graph was drawn. The highest difference between mean drag values in level 4 simulations (with the same turbulent viscosity constant but different time step lengths) is 0.01398 (corresponding to $\nu_{\text{turb}} = 0.01$). However, for choices of the turbulent viscosity constant between 0.03 and 0.1, the difference is

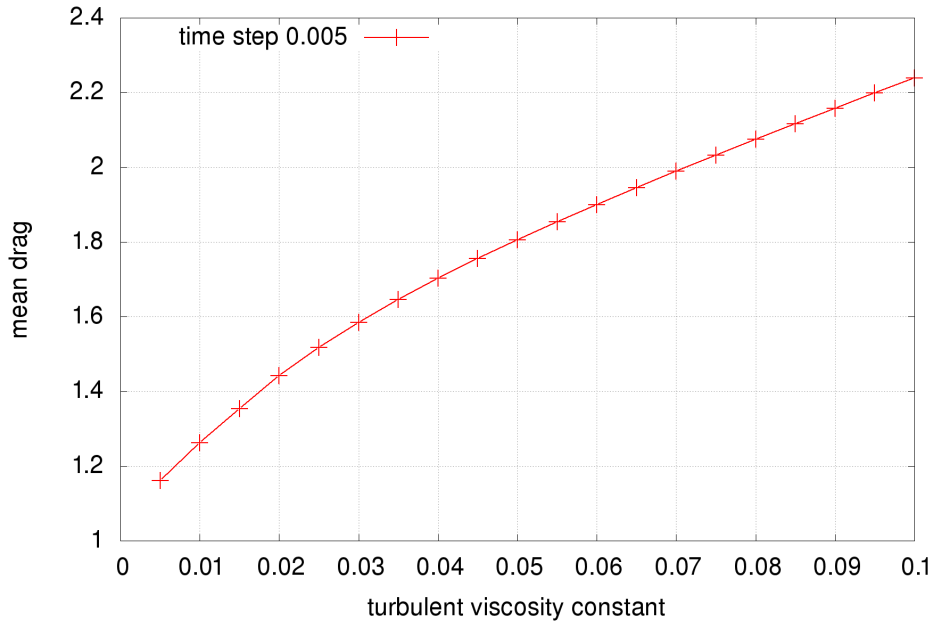

Figure 13: Mean drag values for level 3 simulations. The values for the other time step lengths (0.01 and 0.02) would overlap and were therefore not drawn.

smaller than 0.0015 (see Fig. 14). In essence, the choice of the time step length does not seem important for mean drag values if the turbulent viscosity constant is equal or higher than 0.03.
Figures 15 and 16 show a comparison between level 3 and level 4 simulations. The functions f_1, g_1, f_2 and g_2 were fitted to the respective curves using the nonlinear least-squares Marquardt-Levenberg algorithm. We see an obvious correlation between an increasing turbulent viscosity constant and the mean drag. The level 4 simulations are not that sensitive to the turbulent viscosity constant since the ascend of the lines g_1 and g_2 is smaller than the ascend of the lines f_1 and f_2, respectively.

Level 4		**time step length**		
		0.005	0.010	0.020
turbulent viscosity constant	0.005	1.44942	1.46193	1.46076
	0.010	1.44620	1.44689	1.46018
	0.015	1.43123	1.42604	1.43187
	0.020	1.41012	1.40847	1.40629
	0.025	1.39204	1.39130	1.38867
	0.030	1.38287	1.38245	1.38140
	0.035	1.37536	1.37482	1.37564
	0.040	1.37752	1.37699	1.37716
	0.045	1.38623	1.38580	1.38593
	0.050	1.39810	1.39766	1.39774
	0.055	1.41147	1.41099	1.41101
	0.060	1.42584	1.42535	1.42539
	0.065	1.44092	1.44043	1.44042
	0.070	1.45640	1.45592	1.45587
	0.075	1.47209	1.47160	1.47156
	0.080	1.48783	1.48734	1.48729
	0.085	1.50356	1.50307	1.50301
	0.090	1.51921	1.51873	1.51864
	0.095	1.53476	1.53427	1.53420
	0.100	1.55018	1.54968	1.54874

Table 3: Mean drag values for level 4 simulations. The data is visualized in Fig. 14.

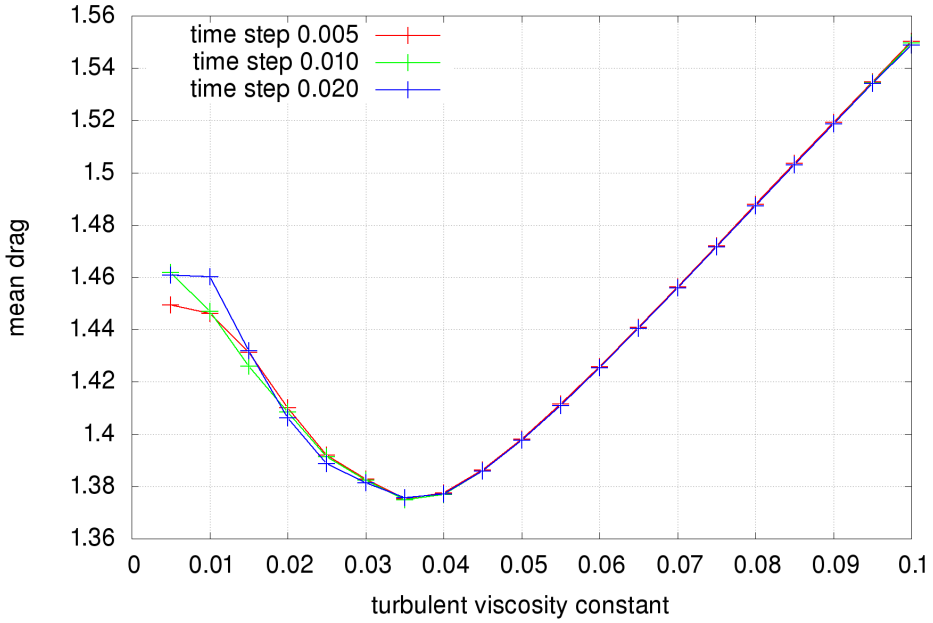

Figure 14: Mean drag values for level 4 simulations.

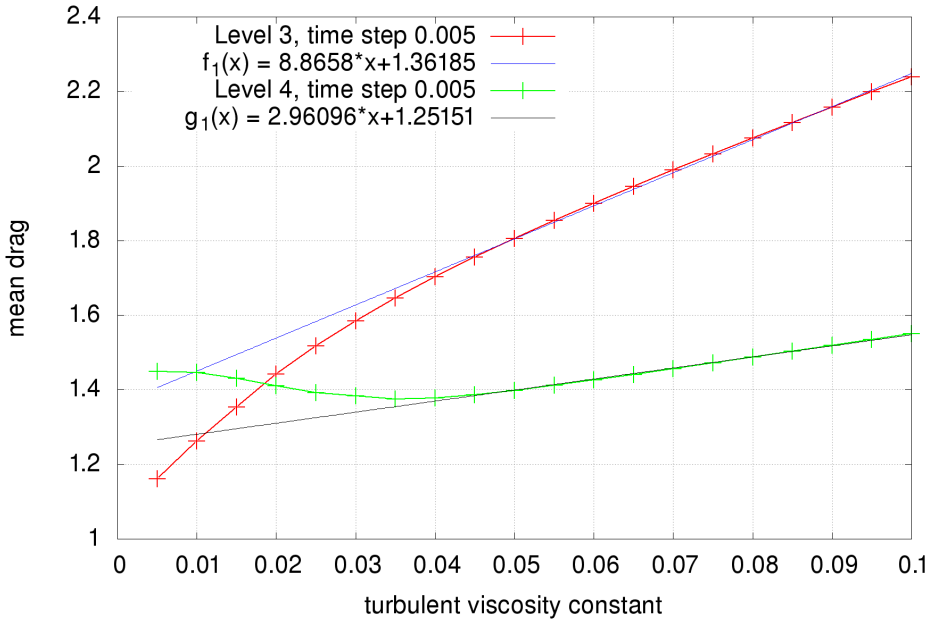

Figure 15: A comparison between level 3 and level 4 simulations. The least-square lines (blue and black) were fitted to the interval [0.04,0.1] of the respective curve.

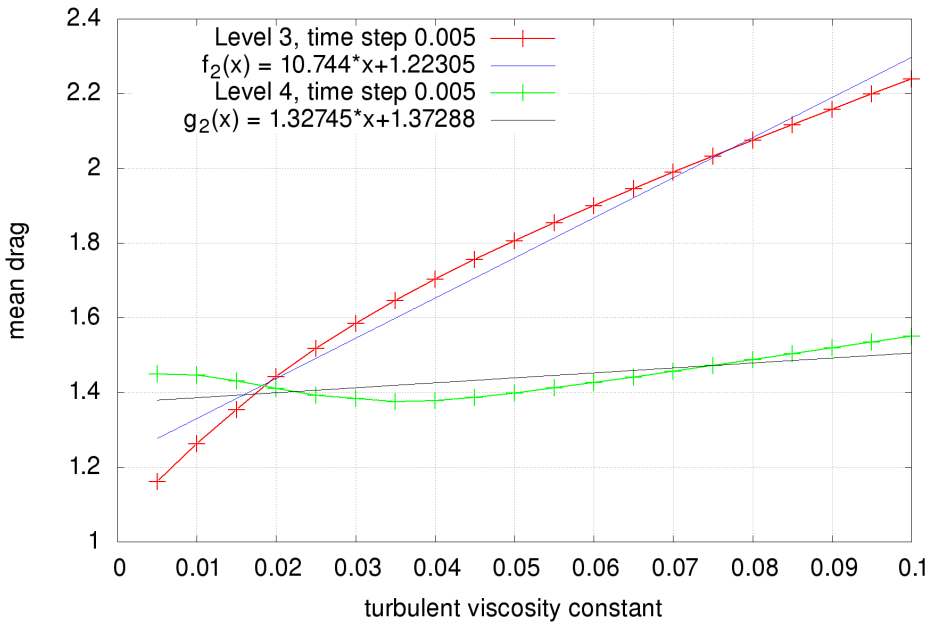

Figure 16: A comparison between level 3 and level 4 simulations. The least-square lines (blue and black) were fitted to the whole interval of the respective curve.

3.3.2 Comparison with other studies

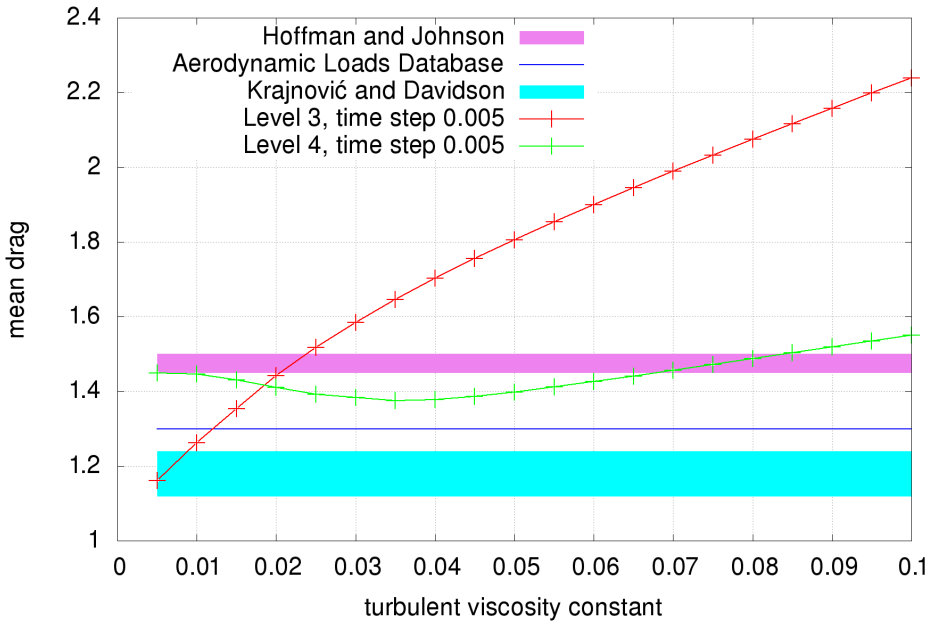

Figure 17: A comparison between the sources. Note that the values from the database and from Krajnović and Davidson are not corresponding to the problem described in Section 3.1 (see quotes).

Hoffman and Johnson [24] calculated mean drag coefficients for the same problem. They used adaptive DNS/LES, a method that refines the grid, thus increasing the number of mesh points.
Hoffman and Johnson [24, pp. 3-4] report:

> We find that $c_{\text{drag}} = 1.48$ using about 400 000 mesh points in space. The only other result (!) available in the literature seems to be that of [25], where values in the range $c_{\text{drag}} = 1.12 - 1.24$ are presented. Surprisingly, no measurements seem to be available, maybe because of lacking motivation because of lacking computations and little interest from the car industry in cubic vehicles. A measured value of $c_{\text{drag}} = 1.3$ is reported [26] for a box with height-width ratio 5 : 1. It seems very likely that the c_{drag} for a cube would be larger than that for a more slender box.[5]

Their value of $c_{\text{drag}} = 1.48$ seems to fit well with our data from level 4 simulations. The values of Krajnović and Davidson [25] only compare to

[5] The references and the variable name in the quote were adjusted to reflect this thesis' reference list and nomenclature.

values we gained from level 3 simulations with very low turbulent viscosity constant (less than 0.01).
Hoffman and Johnson [24, p. 12] define the mean drag coefficient over the time interval $I = [0, 4]$ at fully developed flow as

$$\bar{c}_{\text{drag}} = \frac{1}{|I|} \int_I c_{\text{drag}}(t)\, dt, \qquad \bar{c}_{\text{lift}} = \frac{1}{|I|} \int_I c_{\text{lift}}(t)\, dt. \tag{3.13}$$

Hoffman and Johnson [24, p. 8] report:

> In Figure 3.2 we show the computed values of $\bar{c}_{\text{drag}}$ (for a time interval of length $40H$). The approximations of $\bar{c}_{\text{drag}}$ approaches $1.45 - 1.5$, a value that is well captured already using less than 10^5 mesh points.
>
> We know of no experimental reference values of $\bar{c}_{\text{drag}}$, but in [25] $\bar{c}_{\text{drag}}$ is approximated computationally. The computational setup is similar to the one in this paper except the numerical method, a different length of the time interval, and that we in this paper use a channel of length $15H$, compared to a channel of length $10H$ in [25]. Using different meshes and subgrid models, approximations of $\bar{c}_{\text{drag}}$ in the interval $[1.14, 1.24]$ are presented in [25].[6]

See Fig. 17 for a comparison of the mean drag coefficients obtained by Hoffman and Johnson and the MooNMD simulation. The results from the database and from Krajnović and Davidson are included, but they correspond to similar, but different problems. The level 4 simulations support the values obtained by Hoffman and Johnson, especially at a turbulent viscosity constant around 0.075. The difference of mean drag values is at most about 0.075 at turbulent viscosity constant 0.035.

[6] The references and the variable names in the quote were adjusted to reflect this thesis' reference list and nomenclature.

4 Conclusion

The Smagorinsky model is a very useful model since it is well understood analytically and produces reasonable results, as seen with the level 4 simulations (Fig. 17).
It is clear that more data on the mean drag coefficients is needed, since there are only three results. Since Krajnović and Davidson analyzed a slightly different problem, it further complicates things.
From Fig. 17 it is clear that level 4 simulations are far superior to level 3 simulations over a wide range of turbulent viscosity constants, as they closely align to the data collected by Hoffman and Johnson.
In both level 3 and 4 simulations, the mean drag values are linearly correlated with the turbulent viscosity constant. The values obtained from level 3 simulations are much more sensitive with a slope of about 10.7 versus 1.3 (see Fig. 16).

5 Appendix

5.A Derivation of the filtered momentum equation

The following is adapted from [1, pp. 16f. and 581f.]. When we filter the momentum equation (Eq. (1.2)), we get (since differentiating and filtering commutes and linearity applies):

$$\partial_t \overline{u}_j + \overline{u_i \partial_i u_j} = 2\nu \partial_i \overline{S}_{ij} - \frac{1}{\rho}\partial_j \overline{P} + \overline{f}_j \qquad \text{in } \Omega \times (0,T], \qquad j = 1,2,3.$$

We define the residual-stress tensor, anisotropic residual-stress tensor and modified filtered pressure:

$$\tau_{ij}^R := \overline{u_i u_j} - \overline{u}_i \overline{u}_j, \tag{5.1}$$

$$\tau_{ij}^r := \tau_{ij}^R - \frac{1}{3}\tau_{kk}^R \delta_{ij}, \tag{5.2}$$

$$\bar{p} := \frac{1}{\rho}\overline{P} + \frac{1}{3}\tau_{kk}^R. \tag{5.3}$$

By using the continuity equation (Eq. (1.3)) and filtered continuity equation (Eq. (2.2)), we get

$$\partial_i(u_i u_j) = (\partial_i u_i)u_j + u_i \partial_i u_j = u_i \partial_i u_j, \tag{5.4}$$

$$\partial_i(\overline{u}_i \overline{u}_j) = (\partial_i \overline{u}_i)\overline{u}_j + \overline{u}_i \partial_i \overline{u}_j = \overline{u}_i \partial_i \overline{u}_j. \tag{5.5}$$

Using the last two equations and the definition of the residual-stress tensor τ_{ij}^R, we obtain

$$\begin{aligned}
\partial_t \overline{u}_j + \overline{u_i \partial_i u_j} &= \partial_t \overline{u}_j + \overline{\partial_i(u_i u_j)} \\
&= \partial_t \overline{u}_j + \partial_i(\overline{u_i u_j}) \\
&= \partial_t \overline{u}_j + \partial_i(\overline{u}_i \overline{u}_j) + \partial_i \tau_{ij}^R \\
&= \partial_t \overline{u}_j + \overline{u}_i \partial_i \overline{u}_j + \partial_i \tau_{ij}^R.
\end{aligned}$$

Now using all three definitions from above, we get

$$\begin{aligned}
-\partial_i \tau_{ij}^R - \frac{1}{\rho}\partial_j \overline{P} &= -\partial_i \tau_{ij}^r - \partial_i \frac{1}{3}\tau_{kk}^R \delta_{ij} - \frac{1}{\rho}\partial_j \overline{P} \\
&= -\partial_i \tau_{ij}^r - \partial_j \frac{1}{3}\tau_{kk}^R - \frac{1}{\rho}\partial_j \overline{P} \\
&= -\partial_i \tau_{ij}^r - \partial_j \left(\frac{1}{\rho}\overline{P} + \frac{1}{3}\tau_{kk}^R \right) \\
&= -\partial_i \tau_{ij}^r - \partial_j \bar{p}.
\end{aligned}$$

Thus, the filtered momentum equation can be expressed as:

$$\partial_t \overline{u}_j + \overline{u}_i \partial_i \overline{u}_j = \partial_i \left(2\nu \overline{S}_{ij} - \tau_{ij}^r \right) - \partial_j \bar{p} + \overline{f}_j, \qquad j = 1,2,3.$$

5.B Vector spaces

The Lebesgue space $L^p(\Omega)$, $p \in [1,\infty]$, is the Banach space of measurable functions $\mathbf{v}$ on Ω which satisfy

$$\begin{aligned} \|\mathbf{v}\|_{L^p(\Omega)} &:= \left(\int_\Omega |\mathbf{v}(\mathbf{x})|^p \, d\mathbf{x}\right)^{1/p} < \infty \quad \text{if } p \in [1,\infty), \\ \|\mathbf{v}\|_{L^\infty(\Omega)} &:= \operatorname*{ess\,sup}_{\mathbf{x}\in\Omega} |\mathbf{v}(\mathbf{x})| < \infty \qquad\qquad \text{if } p = \infty. \end{aligned} \tag{5.6}$$

For $p = 2$, the Lebesgue space is also a Hilbert space with the scalar product

$$(\mathbf{v}, \mathbf{w}) = \int_\Omega \mathbf{v}(\mathbf{x}) \cdot \mathbf{w}(\mathbf{x}) \, d\mathbf{x}.$$

For one-dimensional functions, the dot represents simple multiplication. Otherwise it represents the dot product for vectors or Frobenius inner product for matrices. For two matrices $A = (a_{ij})_{1\le i,j\le 3}$ and $B = (b_{ij})_{1\le i,j\le 3}$, the Frobenius inner product is

$$A : B := a_{ij} b_{ij}.$$

We write $L^p\,(a,b;V)$ for the Lebesgue space of functions from the interval (a,b) to the Banach space V. The same kind of notation is used for respective Sobolev spaces.
The Sobolev space $W^{m,p}$ is the Banach space of functions for which

$$\begin{aligned} \|\mathbf{v}\|_{W^{m,p}} &:= \left(\sum_{0\le|\alpha|\le m} \|D^\alpha \mathbf{v}\|^p_{L^p(\Omega)}\right)^{1/p} < \infty \qquad \text{if } p \in [1,\infty), \\ \|\mathbf{v}\|_{W^{m,\infty}} &:= \max_{0\le|\alpha|\le m} \|D^\alpha \mathbf{v}\|_{L^p(\Omega)} < \infty \qquad\qquad \text{if } p = \infty \end{aligned}$$

holds true, i.e. it can be defined as

$$W^{m,p}(\Omega) = \left\{\mathbf{v} \in L^p(\Omega) : D^\alpha \mathbf{v} \in L^p(\Omega) \;\forall\, |\alpha| \le m\right\}. \tag{5.7}$$

Let

$$W^{1,3}_{0,div}(\Omega) := \left\{\mathbf{v} \in W^{1,3}(\Omega) : \mathbf{v}|_\Gamma = \mathbf{0},\ \nabla\cdot\mathbf{v} = 0 \text{ in } \Omega\right\} \tag{5.8}$$

be the divergence-free Sobolev space where functions vanish on the boundary $\Gamma = \partial\Omega$,

$$H^1\left(0,T;L^2(\Omega)\right) := W^{1,2}\left(0,T;L^2(\Omega)\right)$$

a Sobolev space that is also a Hilbert space and

$$V := H^1\left(0,T;L^2(\Omega)\right) \cap L^3\left(0,T;W^{1,3}_{0,div}(\Omega)\right) \tag{5.9}$$

a Banach space with the norm

$$\|\mathbf{v}\|_V = \|\nabla \mathbf{v}\|_{L^3(0,T;L^3(\Omega))} + \|\partial_t \mathbf{v}\|_{L^2(0,T;L^2(\Omega))}.$$

For Section 2.7, we also need the vector spaces

$$X := W_0^{1,3}(\Omega) = \left\{ \mathbf{v} \in W^{1,3} : \mathbf{v}|_\Gamma = \mathbf{0} \right\}, \tag{5.10}$$

$$Q := L_0^2(\Omega) := \left\{ q \in L^2(\Omega) : \int_\Omega q \, d\mathbf{x} = 0 \right\}. \tag{5.11}$$

5.C Inlet velocity profile

The following code is from the implementation of the wall-mounted cube problem. Depending on $z = x_3$ and independent of $y = x_2$, the velocity is interpolated from specific values. The inlet velocity is perturbed with white noise, i.e. a small random number is added to each value.

```
176   double um[65] = {
177     0,
178     0.2166,
179     0.6292,
180     0.6926,
181     0.7307,
182     0.7671,
183     0.7941,
184     0.8191,
185     0.8466,
186     0.8716,
187     0.8931,
188     0.9168,
189     0.9367,
190     0.9586,
191     0.9787,
192     0.9986,
193     1.0153,
194     1.0315,
195     1.0461,
196     1.0587,
197     1.0661,
198     1.0723,
199     1.0770,
200     1.0813,
201     1.0843,
202     1.0868,
203     1.0890,
204     1.0890,
205     1.0890,
206     1.0890,
207     1.0900,
```

```
208       1.0930,
209       1.0930,
210       1.0930,
211       1.0928,
212       1.0924,
213       1.0921,
214       1.0911,
215       1.0898,
216       1.0885,
217       1.0869,
218       1.0835,
219       1.0796,
220       1.0747,
221       1.0679,
222       1.0606,
223       1.0527,
224       1.0388,
225       1.0222,
226       1.0083,
227       0.9871,
228       0.9654,
229       0.9445,
230       0.9229,
231       0.9029,
232       0.8814,
233       0.8622,
234       0.8360,
235       0.8091,
236       0.7851,
237       0.7582,
238       0.7199,
239       0.6857,
240       0.4141,
241       0.1327};
242     double noise=0.1, z0, z1, h;
243     int i;
244
245     if ((fabs(x)<1e-6))
246     {
247       // compute lower index for z value
248       i = (int)(320*z);
249       // linear interpolation
250       if (i<64)
251       {
252         z0 = i / 320.0;
253         z1 = (i+1)/320.0;
254         h = z1 - z0;
255         value = (z1 -z)*um[i] + (z-z0) * um[i+1];
256         value /= h;
```

```
257       }
258       else
259         value = um[i];
260       // add noise
261       if ((fabs(z)>1e-6)&&((fabs(z-0.2)>1e-6)))
262         value += noise * ((double)rand()/RAND_MAX-0.5);
263     }
264     else
265     {
266       value = 0;
267     }
```

Nomenclature

Upper-case Roman

A constant in the derivation of the Smagorinky model (Eq. (2.8))

C_S Smagorinsky coefficient (Eq. (2.12))

$\widetilde{C}_S$ Smagorinsky parameter (see Section 2.4)

$E(k)$ energy spectrum function (Eq. (2.6))

G_Δ filter function (Section (2.1))

F_{drag} drag force (Eq. (3.5))

F_{lift} lift force (Eq. (3.6))

H cube side length in the benchmark problem ($H = L = 0.1\,\text{m}$)

H^1 Sobolev (Hilbert-) space ($H^1 := W^{1,2}$)

K Kolmogorov constant related to $E(k)$ (Eq. (2.6))

$\mathbb{K}_{ij}$ subtest-scale stress tensor (Eq. (2.15))

$\mathbb{L}_{ij}$ Germano identity (Eq. (2.16))

L characteristic length

L^p Lebesgue space (Eq. (5.6))

P pressure

Q vector space (Eq. (5.11))

Re Reynolds number (Eq. (1.1))

S_{ij} rate-of-strain tensor (or velocity deformation tensor, Eq. (1.4))

$\overline{S}_{ij}$ filtered rate-of strain tensor (Eq. (2.3))

$\mathbb{S}_{ij}$ stress tensor (Eq. (3.2))

U characteristic velocity

V vector space (Eq. (5.9))

$W^{m,p}$ Sobolev space (Eq. (5.7))

$W^{1,3}_{0,div}$ divergence-free Sobolev space where functions vanish on the boundary (Eq. (5.8))

X vector space defined in Eq. (5.10)

Lower-case Roman

c_{drag} drag coefficient (Eq. (3.7))

$\bar{c}_{\text{drag}}$ mean drag coefficient (Eq. (3.13))

c_{lift} lift coefficient (Eq. (3.7))

$\bar{c}_{\text{lift}}$ mean lift coefficient (Eq. (3.13))

$\mathbf{f} = (f_1, f_2, f_3)^T$ forces per unit mass acting on the fluid

ℓ_S Smagorinsky lengthscale ($\ell_S = C_S\Delta$)

$\mathbf{n} = (n_1, n_2, n_3)^T$ outward unit surface normal to $\Gamma = \partial\Omega$

$\hat{p}$ dimensionless pressure (Eq. (3.4))

$\bar{p}$ modified filtered pressure (Eq. (5.3))

Upper-case Greek

Γ boundary of the domain ($\Gamma = \partial\Omega$)

Γ_{cube} surface of the cube

Δ filter width

$\widehat{\Delta}$ test filter (Section 2.4)

Ω domain

Lower-case Greek

ε kinetic energy dissipation rate by viscous effects (Eq. (2.7))

$\tilde{\varepsilon}$ kinetic energy transfer rate through the cutoff (a specific wave number)

ε_I injection rate of turbulent kinetic energy into the flow (Eq. (2.11)))

μ dynamic viscosity in $\text{kg}/(\text{m} \cdot \text{s})$

ν kinematic viscosity ($\nu = \mu/\rho\,[\text{m}^2/\text{s}]$)

ν_r residual subgrid-scale eddy viscosity (Eq. (2.5))

ν_{turb} turbulent viscosity constant (Eq. (3.1))

ρ density in kg/m^3

τ_{ij}^R residual-stress tensor (or Reynolds stress tensor, Eq. (5.1))

τ_{ij}^r anisotropic residual-stress tensor (Eq. (5.2), see also Eq. (2.4))

Abbreviations

DNS direct numerical simulation

EDQNM eddy-damped quasinormal Markovian model (see [15], as cited in [4, p. 293])

LES large-eddy simulation

MooNMD Mathematics and object oriented Numerics in Magdeburg (a program package, see [21])

NSE Navier-Stokes equations (see Section 1.4)

TFM two-fluid model

References

[1] S. B. Pope, *Turbulent Flows*. Cambridge University Press, 2000.

[2] V. John. (2014). Numerical methods for incompressible flow problems I, [Online]. Available: `http://www.wias-berlin.de/people/john/LEHRE/NUM_NSE_14/script_num_nse_1_2014.pdf`.

[3] J. Hoffman and C. Johnson, "A new approach to computational turbulence modeling", *Comput. Methods in Appl. Mech. Eng.*, vol. 195, pp. 2865–2880, 2006.

[4] P. Sagaut, *Large Eddy Simulation for Incompressible Flows: An Introduction*, J.-J. Chattot, C. A. J. Fletcher, R. Glowinski, W. Hillebrandt, M. Holt, Y. Hussaini, H. B. Keller, J. Killeen, D. I. Meiron, M. L. Norman, S. A. Orszag, K. G. Roesner, and V. V. Rusanov, Eds., ser. Scientific Computation. Berlin, Heidelberg, and New York: Springer-Verlag, 2001.

[5] V. John and W. J. Layton, "Analysis of numerical errors in large eddy simulation", *SIAM J. Numer. Anal.*, vol. 40, no. 3, pp. 995–1020, 2002. [Online]. Available: `http://www.wias-berlin.de/people/john/ELECTRONIC_PAPERS/JL02.SINUM.pdf`.

[6] V. John, *Large Eddy Simulation of Turbulent Incompressible Flows: Analytical and Numerical Results for a Class of LES Models*, T. J. Barth, M. Griebel, D. E. Keyes, R. M. Nieminen, D. Roose, and T. Schlick, Eds., ser. Lecture Notes in Computational Science and Engineering 34. Berlin and Heidelberg: Springer-Verlag, 2004.

[7] L. C. Berselli, T. Iliescu, and W. J. Layton, *Mathematics of Large Eddy Simulation of Turbulent Flows*, J.-J. Chattot, P. Colella, W. E, R. Glowinski, M. Holt, Y. H. P. Joly, H. B. Keller, D. I. Meiron, O. Pironneau, A. Quarteroni, J. Rappaz, R. Rosner, J. H. Seinfeld, A. Szepessy, and M. F. Wheeler, Eds., ser. Scientific Computation. Berlin and Heidelberg: Springer-Verlag, 2006.

[8] Y. Zang, R. L. Street, and J. R. Koseff, "A dynamic mixed subgrid-scale model and its application to turbulent recirculating flows", *Phys. Fluids A*, vol. 5, pp. 3186–3196, 1993.

[9] J. H. Ferziger and M. Perić, *Computational Methods for Fluid Dynamics*, 3rd ed. Berlin, Heidelberg, and New York: Springer-Verlag, 2002. [Online]. Available: `http://user.uni-frankfurt.de/~shahraki/index_htm_files/Ferziger%20Peric%20-%20Computational%20Methods%20for%20Fluid%20Dynamics,%203rd%20Ed%20-%202002.pdf`.

[10] A. N. Kolmogorov, "The local structure of turbulence in incompressible viscous fluids for very large Reynolds number", *Dokl. Akad. Nauk SSR*, vol. 30, pp. 9–13, 1941.

[11] B. Aupoix and J. Cousteix, "Modèles simples de tensions de sous-maille en turbulence homogène isotrope", French, *Rech. Aéro.*, vol. 4, pp. 273–283, 1982.

[12] M. Germano, U. Piomelli, P. Moin, and W. H. Cabot, "A dynamic subgrid scale eddy viscosity model", *Phys. Fluids A*, vol. 3, pp. 1760–1765, 1991. [Online]. Available: `http://dx.doi.org/10.1063/1.857955`.

[13] D. K. Lilly, "A proposed modification of the germano subgrid-scale closure method", *Phys. Fluids A*, vol. 4, pp. 633–635, 1992. [Online]. Available: `http://dx.doi.org/10.1063/1.858280`.

[14] M. Breuer, "Large eddy simulation of the subcritical flow past a circular cylinder: numerical and modeling aspects", *Int. Jour. Num. Meth. Fluids*, vol. 28, pp. 1281–1302, 1998. [Online]. Available: `http://citeseerx.ist.psu.edu/viewdoc/download?doi=10.1.1.465.4731&rep=rep1&type=pdf`.

[15] M. Lesieur, *Turbulence in Fluids*, 3rd ed., ser. Fluid Mechanics and its Applications. Kluwer Academic Publishers, 1997, vol. 40.

[16] O. Ladyzhenskaya, "New equations for the description of motion of viscous incompressible fluids and solvability in the large of boundary value problems for them", *Proc. Steklov Inst. Math.*, vol. 102, pp. 95–118, 1967.

[17] ——, *The Mathemetical Theory of Viscous Incompressible Flow*, 2nd ed. New York, London, and Paris: Gordon and Breach, 1969.

[18] Q. Du and M. D. Gunzburger, "Finite-element approximations of a Ladyzhenskaya model for stationary incompressible viscous flow", *SIAM J. Numer. Anal.*, vol. 27, no. 1, pp. 1–19, Feb. 1990.

[19] J. Hoffman, "Computation of mean drag for bluff body problems using adaptive dns/les", *SIAM J. Sci. Comput.*, vol. 27, no. 1, pp. 184–207, 2005. [Online]. Available: `http://epubs.siam.org/doi/pdf/10.1137/040614463`.

[20] W. Rodi, J. H. Ferziger, M. Breuer, and M. Pourquie, "Status of large eddy simulation: results of a workshop", *ASME J. Fluids Engrg*, vol. 119, pp. 248–262, 1997. [Online]. Available: `http://www.ewp.rpi.edu/hartford/~ernesto/F2012/CFD/Readings/Rodi1997.pdf`.

[21] V. John and G. Matthies, "MooNMD – a program package based on mapped finite element methods", *Computing and Visualization in Science*, vol. 6, pp. 163–170, Mar. 2004. [Online]. Available: `http://link.springer.com/content/pdf/10.1007%2Fs00791-003-0120-1.pdf`.

[22] V. John, "On the efficiency of linearization schemes and coupled multigrid methods in the simulation of a 3d flow around a cylinder", *Int. J. Numer. Meth. Fluids*, vol. 50, pp. 845–862, 2006.

[23] V. John, G. Matthies, and J. Rang, "A comparison of time-discretization/linearization approaches for the incompressible navier-stokes equations", *Comput. Methods Appl. Mech. Engrg.*, vol. 195, pp. 5995–6010, 2006.

[24] J. Hoffman and C. Johnson, "Adaptive dns/les: a new agenda in cfd", in *Finite Element Methods: 1970s and beyond*, L. Franca, T. Tezduyar, and A. Masud, Eds., CIMNE, 2004. [Online]. Available: `http://www.nada.kth.se/~jhoffman/archive/papers/adnsles.pdf`.

[25] S. Krajnović and L. Davidson, "Large-eddy simulation of the flow around a bluff body", *AIAA Journal*, vol. 40, no. 5, pp. 927–936, May 2002. [Online]. Available: `http://arc.aiaa.org/doi/pdf/10.2514/2.1729`.

[26] (n.d.). Aerodynamic loads database. Moved from the previous URL (`http://www.nd.edu/~nathaz/database/`), [Online]. Available: `http://aerodata.ce.nd.edu`.